

Diss. ETH No. 5985

LASER-GENERATED STRESS WAVES IN LIQUIDS

A dissertation submitted to the
SWISS FEDERAL INSTITUTE OF TECHNOLOGY, ZURICH

for the degree of
Doctor of Natural Sciences
presented by

M A R K U S W. S I G R I S T

Dipl. Phys. ETHZ

born September 6, 1948

citizen of Rafz (Canton Zurich)

accepted on the recommendation of

Prof. Dr. F.K. Kneubühl

Prof. Dr. H.P. Weber (University of Berne)

1 9 7 7

ABSTRACT

The features of the laser-induced stress generation in liquids by the vaporization process and the thermoelastic effect are presented.

In the first part, the devices used for the investigations are described. Subsequently, the experimental results obtained for water, n-heptane and carbon tetrachloride are discussed. For the first time, the individual contributions of the vaporization and of the thermoelastic effect on the stress generation are outlined in detail. Most important for the phenomenon of generation of the stress waves is the amount of the absorbed laser energy density in comparison to the vaporization threshold of the liquid. Furthermore, the influence of the laser pulse characteristics is emphasized for the example of tunable high-frequency acoustic waves. These waves are generated by the impact of a self mode-locked laser pulse. The phenomenon of pressure saturation with increasing laser peak power, observed in CCl_4 , could be explained by a reduced absorptivity at higher laser power.

Since existing theories on the thermoelastic generation of acoustic waves do not yield satisfactory agreement with our experimental data, we propose a new spherical model, which is presented in the second part. In this model the transient heating caused by the laser impact, is represented by the three-dimensional heat pole. An analytical solution of the thermoelastic pressure wave is derived. Its good agreement with the experiment is discussed.

ZUSAMMENFASSUNG

In dieser Arbeit werden die Merkmale der Erzeugung von Stosswellen in Flüssigkeiten durch Lasereinschuss diskutiert, wobei das Hauptgewicht auf den Verdampfungsprozess und den thermoelastischen Effekt gelegt wird. Im ersten Teil werden die für die Untersuchungen benutzten Geräte beschrieben. Anschliessend folgt eine Diskussion der experimentellen Resultate für Wasser, n-Heptan und Tetrachlorkohlenstoff. Die individuellen Beiträge der Verdampfung und des thermoelastischen Effektes zur Erzeugung von Stosswellen werden dabei zum ersten Mal im Detail veranschaulicht. Als wichtigster Parameter für die Stosswellenerzeugung erweist sich der Betrag der absorbierten Laserenergiedichte im Vergleich zur Verdampfungsschwelle der Flüssigkeit. Im weiteren wird der Einfluss der zeitlichen Struktur des Laserimpulses am Beispiel hochfrequenter Schallwellen mit abstimmbarer Frequenz hervorgehoben. Diese Wellen werden durch den Einschuss mit einem selbst modengekoppelten Laserimpuls erzeugt. Das Phänomen der Drucksättigung mit steigender Laserleistung, das in CCl_4 beobachtet wurde, konnte mit einer reduzierten Absorption bei höherer Laserleistung erklärt werden.

Da bestehende Theorien über die thermoelastische Erzeugung von Schallwellen keine befriedigende Uebereinstimmung mit unseren experimentellen Daten ergeben, schlagen wir im zweiten Teil ein neues, sphärisches Modell vor. In diesem Modell wird die schlagartige Aufheizung, wie sie durch den Lasereinschuss erzeugt wird, durch den dreidimensionalen Wärmepol dargestellt. Eine analytische Lösung für die thermoelastische Druckwelle wird hergeleitet. Die gute Uebereinstimmung mit dem Experiment wird abschliessend diskutiert.

PART I: EXPERIMENTAL STUDIES

I. INTRODUCTION

The generation of sound by the absorption of laser radiation in a liquid was first reported by Askar'yan [1] . Since then many investigations of this effect have been performed, both experimentally and theoretically.

Hu [2] proposed four mechanisms responsible for the stress production in liquids by laser impact, i.e. dielectric breakdown, electrostriction, vaporization and thermoelastic process. In comparison with these four interaction mechanisms, the radiation pressure is negligible [3] .

The dielectric breakdown is the most efficient mechanism for stress generation. It can be realized even in transparent media, where the sound generation due to the ordinary absorption does not occur. However, the threshold intensity for inducing breakdown in pure liquids is high. Barnes [4] found, that a laser intensity of approximately $5 \cdot 10^{11} \text{ W cm}^{-2}$ is necessary to induce breakdown in well filtered water by the impact of a Q-switched ruby laser pulse.

Hence, micron size particles and dissolved air in the liquid have the effect of lowering this threshold drastically [5, 6, 7] . Hitherto, no physical model has been established for this breakdown, although self-focusing or beam trapping have been examined as possible explanations [8] . The laser-induced breakdown in a liquid is manifested by a bright plasma which is accompanied by a shock wave. For the high laser intensities at and below the breakdown threshold, stimulated Brillouin scattering has been observed [4, 9, 10] . This scattering of light in a medium is due to electrostriction coupling [11] . The electrostriction effect as a stress generating interaction mechanism, is important only for transparent media and for laser intensities that imply an electric field strength of the order of 10^7 V cm⁻¹ .

For absorbing liquids and for laser intensities below the breakdown threshold, the interaction is dominated by the vaporization process and the thermoelastic effect [12,13,14,15,16,17,18] .

The vaporization process and the correlated recoil momentum that acts on the surface of the liquid, are only present if the absorbed laser energy density in the medium exceeds the vaporization threshold of the liquid.

In the absence of vaporization the excitation of sound is due to the thermoelastic process. It is associated to the thermal expansion of a rapidly heated volume of the medium. Efficient thermoelastic sound generation requires short laser pulses with durations in the submicrosecond region.

The individual influences of the vaporization process and the thermoelastic effect on the stress generation, as well as their dependence on the physical properties of the liquid, and on the laser pulse characteristics, have not been examined previously in detail. Therefore, our study is restricted to these mechanisms.

The present investigation has been performed in relation to earlier experiments which have demonstrated that the interaction of laser pulses with solids is enhanced by liquid layers spread on solid surfaces [19,20] .

This phenomenon is the result of the laser-induced stress waves in the liquid layer.

Furthermore, our examinations are considered as a first step in the field of laser-induced chemical reactions in liquids. Today, laser-induced chemistry is a topic of increasing interest. Hitherto, the principal research in this field is concentrated on gases, molecular beams and solid matrices.

Our study demonstrates that for the laser intensities under consideration, the interaction with liquids can be described by the normal optical and thermal properties of the liquid.

On the contrary, for the same laser intensity regime, the interaction with metals is determined by metallurgical phase transitions and by the non-linear effects due to plasma formation. Under the same circumstances, the interaction with insulators is dominated by the dielectric breakdown that is caused by absorbing inclusions [21] .

For our experiments on laser-induced stresses in liquids, we used two complementary devices: a high-speed camera for shadowgraphy, and fast stress transducers, which were developed in our laboratory.

II. HYBRID CO₂ LASER

Our studies used a hybrid 10.6 μm -CO₂-laser, which was constructed following the concept suggested by Gondhalekar and Holzhauer [22] . It consists of a TEA-discharge tube in series with a cw-laser tube, both of which are contained within the same resonator. The resistor-pin electrodes of the TEA section are arranged in the usual double helix. As an active gas we choose the mixture He : CO₂ : N₂ = 86:10:4 vol. % at 1 atm . If the TEA section is run without the cw section it provides mode-locked pulses of approximately 150 ns FWHM . The cw-section is operated at 10 torr . Its maximum cw-output is 1 W . In hybrid operation this section is run slightly above the laser threshold. Under this condition the output of the hybrid laser is a smooth pulse without axial mode beating. Typical pulses are shown in the upper traces of Figs. 7 a to 7 c . The average peak power of a pulse is 600 kW , and the half width is 300 ns . At the focus of a Ge lens with $f = 20$ cm a peak intensity of $5 \cdot 10^8 \text{ W cm}^{-2}$ is achieved. Single longitudinal-mode operation is required for reproducible measurements of laser-induced effects in liquids.

According to Girard [23] longitudinal-mode selection in the hybrid laser is obtained by the additional gain of a selected mode, which is provided by the cw-section.

The wavelengths of the pulsed emissions of our hybrid laser were checked with a spectrum analyzer (Optical Engineering, Inc., Model 16-A). We noticed that the laser output accidentally jumped between various molecular transitions of a branch of the 10.4 μm band, e.g. between P (18) and P (20) . Simultaneous observation of the transverse mode structure of the laser beam indicated that a change of the molecular transition is accompanied by a change of the mode pattern. An example is given in Fig. 1 showing the two different mode patterns of adjacent P transitions. This phenomenon is explained in a review by Patel [24, p. 65] . It is due to the composition of our hybrid laser system, which gives rise to strong competition among the molecular transitions. In order to avoid this undesirable effect we replaced the totally reflecting mirror by a diffraction grating blazed at 10.6 μm wavelength. By introducing a limiting aperture inside the cavity the TEM_{00} mode was favoured. The grating and the aperture reduced the laser peak power by a factor of 4 .

III. HIGH-SPEED PHOTOGRAPHY OF LASER-INDUCED STRESS WAVES

A. Purpose

High-speed photography has been widely used for the study of stress-wave generation in liquids by laser impact [5, 6, 7, 14,15,16,25,26,27] . Most of these investigations deal with the dielectric breakdown and the subsequent shock formation, in liquids that are transparent at the wavelength of the incident laser radiation [5, 6, 7, 26,27] . However, for absorbing liquids, and for laser intensities below the breakdown threshold of the liquid, only a few studies have been published [14,15,16,25] . The aim of our photographic investigations was to obtain an insight into the dependence of the geometry of the laser-induced stress waves upon the optical properties of the liquid. A knowledge of the geometry of the pressure transients is required for interpreting the stress measurements with transducers, as well as for experimental examination of theoretical models. Therefore, we studied the laser-generated stress waves in a number of pure liquids with a wide gamut of absorption coefficients α at 10.6 μm wavelength. The absorption coefficients for the liquids employed in these experiments are listed in Table I . They are taken from standard infrared spectra with the exception of the absorption in water [28] .

B. Experimental arrangement

Our studies were performed mainly with shadowgraph techniques [15] using a xenon flashlamp as a light source, and an image converter camera (Hadland Photonics Ltd) that was operated in the framing mode [16] . The laser impact was generated with the aid of the hybrid CO₂-laser that is described in Chapter II . In general, the laser beam was focussed perpendicular with respect to the free surface of the liquid, which was contained in a cuvette at room temperature.

C. Results

The results confirm that the geometry of the laser-induced stress wave is determined by the absorption coefficient α of the liquid. For liquids with a high absorption coefficient $\alpha \geq 25 \text{ cm}^{-1}$, only a hemi-spherical wave is generated, as is illustrated in Fig. 2a. This shows the wave in distilled water 1.8 μs after the impact. We found that a precise hemi-spherical shock front is achieved only with the TEM₀₀ laser mode. With poor mode quality flat shock fronts are obtained, which is in agreement with the observations of Bell and Maccabee [15] .

For liquids with low absorption coefficients $\alpha \leq 25 \text{ cm}^{-1}$ a cylindrical wave [16] is induced, in addition to the hemi-spherical wave. As an example we show in Fig. 2 b the two shock waves in n-pentane 3.5 μs after impact. The center of the hemi-spherical wave corresponds to the impact of the laser beam on the surface of the liquid, whereas the axis of the cylindrical wave is defined by the penetrating laser beam. We were able to confirm this statement concerning the cylindrical wave by directing the laser beam on CCl_4 at an angle of incidence of 40° . The direction of the axis of the observed cylindrical wave obeyed Snell's law.

Laser-induced weak acoustic transients of cylindrical geometry, yet without an indication of the hemi-spherical waves, have been reported previously by Carome et al. [7] and by Longaker et al. [29]. Carome's experiment was performed with a Q-spoiled ruby laser in a filtered solution of benzantracene in benzene. Longaker et al. studied the perturbation of the refractive index interferometrically using the impact of a pulsed Nd-laser in media with different absorptivities.

We found that the width of the disturbance of the refractive index in the shock front of the laser-induced stress-waves is larger for liquids with a lower absorption coefficient α . This phenomenon is obvious when comparing the shock fronts of n-pentane and water shown in Figs. 2 b and 2 a. It is confirmed in detail by our measurements performed with stress transducers (Chapter V) .

The observed penetration depth of the laser beam in liquids with low absorption coefficient α , (e.g. n-pentane, CCl_4) , is considerably larger than $1/\alpha$ [25] , indicating a decrease of α with increasing laser flux. This is in agreement with the stress saturation in CCl_4 discussed in Chapter V .

Furthermore, we observed small bubbles near the laser impact in CCl_4 [25] and in chloroform [30] . These bubbles occur when the rarefaction pulse exceeds the cavitation strength [31] of the liquid. In water the rarefaction is insufficient for the generation of cavitation. This rarefaction wave that follows the compression wave is discussed in Chapter V .

For the first time we found laser-induced breakdown in CS_2 , which is transparent ($\alpha < 1 \text{ cm}^{-1}$) at $10.6 \text{ } \mu\text{m}$.

Fig.2c demonstrates that the impinging laser radiation is partially absorbed at discrete impurity centers where the breakdown and subsequent formation of spherical shock waves occur. Similar investigations were performed with water by Bell and Landt [5] with a ruby laser and by Felix and Ellis [6] with a Nd-laser.

Since the shock-wave velocity is not a sensitive function of the pressure difference across the shock front [32,33], the average wave propagation speeds deduced from the photographs are very close to the proper sound velocity of the liquid. A shock wave velocity above sound speed could be established in CCl_4 on the basis of the geometrical separation of the hemi-spherical from the cylindrical shock front [25].

IV. DEVICES FOR STRESS MEASUREMENTS

A. Purpose

Since both the time dependence and the peak amplitudes of the laser-generated stress transients cannot be determined from shadowgraphs, we developed adequate stress transducers in our laboratory. This allows for the precise measurement of stress transients, and consequently, the deduction of relations between the laser-pulse characteristics, the physical properties of the liquid, and the recorded stress signal.

B. State of the Art

Up to the present various piezoelectric stress transducers have been designed for recording stress waves in solids [34-51] , and in liquids [12,16,52] . Graham and co-workers [34,35,37] developed x-cut quartz gauges operating in the short-circuit mode. The quartz disks of these gauges are manufactured with a thickness of several mm in order to allow a recording time of some 100 ns , and have a diameter of 2 to 3 cm to ensure one-dimensional response. Longer recording times are obtained with the aid of the guard-ring gauge where the piezoelectric current is observed at the inner electrode.

This so-called Sandia-type gauge has been used by many authors [34-48] . A disadvantage of the Sandia-type gauge is its large diameter. This has been pointed out by Krehl et al. [48] . On the other hand, its time resolution is excellent and limited only by the recording instrumentation [34] . Rise times of a few ns [47] or better [42] have been detected. In spite of the large electrode area, the sensitivity of the Sandia-type gauge is typically 1 mV/bar when a 50 Ω shunt resistor is used. Only Bushnell et al. [38] reported considerably higher sensitivity of 76 mV/bar when they used a PZT ceramic.

Bunkin et al. [12] and Lowder et al. [50] constructed gauges which differ from the Sandia type. Whereas Bunkin achieved a sensitivity of only 0.5 to 1 μ V/bar with a spherical receiver, Lowder devised piezoresistive carbon gauges yielding 80 μ V/bar with a sensitive area of only 1.6x1.2 mm² , and a rise time of about 100 ns .

In conclusion, small-electrode gauges of high sensitivity with a recording time of at least 1 μ s and a response time in the ns range are not available at present. Since a small electrode area is required for the detection of spherical waves, we were obliged to develop a new type of pressure gauge for our purpose.

C. Principles of Design

The design of our stress transducers is based on concepts described in the Ph.D. thesis of Meyer [53] . According to Meyer the relation between the voltage $U(t)$ measured over a loading resistor R , and the stress $p(t)$ on the front surface of the piezoelectric disk (e.g. z-cut LiNbO_3) , is given by the following equation

$$U(t) = \frac{Av}{Cd} \cdot \frac{e_{33}}{c_{33}} \cdot \int_0^t [p(0,t') - p(d,t')] \cdot e^{-\frac{t-t'}{\tau}} dt' ,$$

where t = time,

e_{33} = piezoelectric constant of the disk,

c_{33} = modulus of elasticity of the disk,

A = electrode area,

d = thickness of the disk,

v = sound speed of the material of the disk,

C = total capacity of the gauge and the
recording system,

$p(0,t)$ = pressure amplitude on the front surface
of the disk,

$p(d,t)$ = pressure amplitude on the rear surface
of the disk,

$\tau = R \cdot C$ = time constant.

This equation was derived assuming, that the front of the incident shock wave is parallel to the front face of the piezoelectric disk [53] . It can be simplified in four different cases that are defined by different ranges of the stress duration T , the acoustic transit time d/v of the disk, and the time constant τ .

Gauges with thin piezoelectric disks that are run in the open-circuit mode ($\tau \gg T > d/v$) best suit our purpose. In this case the above equation can be simplified to

$$U(t) = \{e_{33} \cdot A / (c_{33} \cdot C)\} \cdot p(0,t) .$$

The output voltage $U(t)$ of the transducer is proportional to the pressure $p(0,t)$ on the front face of the disk. We achieved a high sensitivity $\{e_{33} \cdot A / (c_{33} \cdot C)\}$ by using piezoelectric materials with a large e_{33}/c_{33} ratio, and by reducing C as much as possible under the condition $RC \gg T$. In the design of the gauge the electrode area has to be small in order to avoid distortions caused by the spherical or cylindrical fronts of the shock waves.

In the open-circuit mode the response time of the gauge equals d/v [53] . Therefore, we used thin crystals of material with a high sound speed v , e.g. LiNbO_3 or quartz.

D. Construction

The scheme of a gauge constructed according to the principles stated in Section IV C is shown in Fig. 3 .

The gold-coated piezoelectric crystal is glued with silver-conductive epoxy on the polished front face of a metallic bar that has identical lateral dimensions. The best performance is achieved with z-cut LiNbO_3 crystals. Dimensions are typical 2x2 mm , and a usual thickness is 30 to 80 μm . Since the width-to-thickness ratios of the crystals are well above 10, fully electroded disks can be used instead of the sophisticated guard ring configuration of the Sandia-type gauges (Section IV B) .

In order to avoid reflections at the crystal-bar interface, the metal of the bar was chosen with an acoustic impedance similar to that of the piezoelectric crystal. The front electrode, in direct contact with the liquid, is connected electrically to the coaxial brass holder in which the above assembly is fixed with epoxy resin.

The output of the gauge is connected either directly to the $1\text{ M}\Omega$ input of an oscilloscope (Tektronix 7844), or indirectly with a Tektronix P 6201 FET probe as intermediary. The latter arrangement reduces the input capacity to 3 pF .

Finally, it should be mentioned that the effective pressure in the shock wave is only half the value measured by the gauge, because the acoustic impedance of the liquid is considerably less than that of the piezoelectric disk.

E. Performance

With z-cut LiNbO_3 crystals we achieved in the open-circuit mode sensitivities of the order of 100 mV/bar with corresponding response times between 4 ns and 11 ns . These values are superior to our data published previously [16] , because of an improvement of the crystal geometry and the use of the FET probe.

The sensitivity of our stress transducers is considerably higher than that of the Sandia-type gauges discussed in Section IV B . In contrast to our transducers the Sandia-type gauges are operated in the short-circuit mode, yielding a typical sensitivity of 1 mV/bar for a response time near 1 ns .

Recently, Huff and Graham [52] reported on pressure measurements performed with a LiNbO_3 transducer which was run in the same mode (open-circuit, voltage) as our gauges. This transducer achieved a sensitivity of 2 mV/bar for an unspecified response time.

F. Experimental Arrangement

The experimental arrangement for measurements on laser-induced shock waves in liquids with the aid of stress transducers is shown in Fig. 4 . The laser beam is focused perpendicular to the free surface of the liquid. Part of the beam is deflected by a beam-splitter into a photon drag detector (Rofin Ltd) , with a sensitivity of 0.18 mV/kW , and a response time of less than 1 ns . The liquid is contained in a cell where one stress gauge is placed on the bottom for recording of the hemi-spherical stress transients, and another gauge on the side wall to measure the cylindrical shock waves. The cell is mounted on an xy-positioner which allows adjustment of the position of the stress gauges with respect to the incident laser beam. The dual beam Tektronix 7844 oscilloscope permits simultaneous observation of the laser pulse and the induced stress transient.

The oscilloscope is triggered by the deflected laser pulse. The time delay between the laser pulse and its stress transient represents the acoustic transit time from the laser impact to the stress transducer through the liquid.

V. EXPERIMENTAL RESULTS ON STRESS MEASUREMENTS

A. Survey

As discussed in Chapter I the interaction of laser pulses with absorbing liquids is dominated by the thermoelastic effect, and the vaporization process for the laser intensities under consideration. The following experiments have been performed in order to gain an insight into the individual influences of these two interaction mechanisms, and of the laser pulse characteristics on the stress generation in liquids. The liquids carbon tetrachloride, n-heptane and distilled water have been studied. With respect to our experiments these liquids are mainly characterized by the vaporization threshold, the absorption coefficient α , and the sound attenuation coefficient δ . These and additional data of the three liquids are listed in Table II .

The first experiments were aimed to study the influence of the spatial and temporal structure of the laser pulse on the stress generation (Section V B) . The subsequent investigations have concentrated on examining the dependence of the stress formation on the vaporization threshold of the liquid.

The temporal behaviour of the stress transients has been examined for absorbing energy densities well above (Section V C) , near, (Section V D) , and below (Section V E) the vaporization threshold. This was done in order to distinguish and to characterize the influence of the dominant mechanisms of interaction.

Although the vaporization threshold is higher for water than for n-heptane and CCl_4 , it can be easily surpassed, because of the high absorption coefficient α of water (Table I) . Whereas the maximum laser energy employed for this study is above the threshold energy density of n-heptane, the deposited maximum laser energy density is not sufficient to vaporize CCl_4 . Therefore, a different behaviour of the three liquids under the laser impact is expected. This is described in Sections V C - E where we have emphasized the special effects in water, where the three energy regimes can be adjusted easily.

B. Dependence of the stress generation on the laser pulse characteristics

Since a change of the molecular transition in the laser is correlated to a change in the transverse mode (Fig. 1) , the mode pattern in the laser focus can be varied. The influence of the mode structure of the laser beam on the induced peak stress is shown in Fig. 5 . In this figure the peak stress recorded by the transducer, placed 20 mm below the free surface of the water, is plotted versus the incident laser peak power. The resulting straight curves correspond to two different molecular laser transitions. For identical laser power the stress amplitudes differ by a factor of two. This phenomenon cannot be explained by the negligible difference of the absorption coefficient α for the neighbouring frequencies of the two molecular transitions. The respective frequency separation of approximately 50 GHz is much less than the width of the absorption band of water. Consequently the change of the transverse mode pattern is responsible for the observed drastic difference of the peak stresses. This experiment demonstrates the importance of the mode control and the mode stability for this type of studies. To our knowledge this has not been emphasized hitherto.

Another interesting manifestation of the dependence of the acoustic transients on the structure of the laser pulse, is the generation of high-frequency sound waves by longitudinal mode beating of the laser. If the cw part of the hybrid CO₂ laser is operated at the threshold, the self mode-locked laser pulse consists of a train of single spikes, separated by the resonator round-trip time. The impact of these spikes on water generates acoustic sound waves with frequencies up to 60 MHz , which were detected by our transducers (Chapter IV) . An example with 40 MHz waves is shown in Fig. 6 , where the upper trace represents the laser pulse, and the lower trace the corresponding stress signal. If the absorbed laser energy density is below the vaporization threshold of the liquid, only the thermoelastic process is responsible for sound generation. Under this condition a definite temporal correlation of the laser pulse and the acoustic wave has been detected. This is also found in Fig. 6 where the spike separation of the two traces is identical. It has to be emphasized that the modulation of the pressure pulse recorded can be caused neither by transducer resonances nor by oscillations of laser-induced bubbles within the liquid [26] .

The detected sound frequency is independent of the gauge configuration, and it can be shifted simply by varying the length of the laser resonator.

Our experimental result represents a qualitative verification of a theory of transient heating by White [3] . For the absorption of a harmonically oscillating laser power density, he predicts elastic waves with frequency components primarily associated with the laser pulse envelope, i.e. the spike frequency.

The observed generation of high-frequency acoustic waves demonstrates that the thermoelastic effect (Section V E) is a very fast process. This fact will be taken into account in our theoretical model presented in Part II .

High-frequency acoustic waves have not been detected in all of the three liquids investigated. This is due to the different sound attenuation coefficients δ listed in Table II . This coefficient is proportional to the square of the sound frequency f , within a certain frequency range [54,55] .

Therefore, the high-frequency signals are strongly attenuated in liquids. In water δ/f^2 is approximately $25 \cdot 10^{-17} \text{ s}^2 \text{ cm}^{-1}$ in the MHz range. This yields a decay of the initial peak pressure p_i to $0.7 p_i$ within a distance of 1 cm at 40 MHz. Hence, the pressure spikes can be well observed in water for distances up to 4 cm. In CCl_4 , however, the attenuation of the sound wave is much stronger ($\delta/f^2 = 530 \cdot 10^{-17} \text{ s}^2 \text{ cm}^{-1}$). In consequence, only the average structure-free pulse envelope is observed. In n-heptane the high-frequency pressure oscillations have been detected within a distance of 1 cm, which is in agreement with the calculated attenuation ($\delta/f^2 = 80 \cdot 10^{-17} \text{ s}^2 \text{ cm}^{-1}$).

Finally, we should mention that for the first time high-frequency acoustic waves, generated directly by a single laser beam, have been detected with a piezoelectric transducer in a liquid. Felix [44] reported laser-induced 1 to 25 MHz sound-wave trains in water, that are generated by an indirect sandwich technique. The technique shows a much lower efficiency than the direct method.

Brienza et al.[56] demonstrated the possibility of generating microwave sound by surface heating of a thin metallic film with a mode-locked Nd: glass laser. In a recent paper by von Gutfeld et al.[57] the production of 20 MHz acoustic waves in solids by pulsed optical or electrical excitation was discussed. Enhanced amplitudes were achieved using constrained surfaces.

C. Effects for laser energies above the vaporization threshold

For absorbed laser-energy densities well above the vaporization threshold of the liquid, the interaction is dominated by the vaporization process. High-speed photography shows that this process lasts several ms . The vapor escapes mainly normal to the liquid surface. A recoil momentum equal to the momentum of the vapor acts on the surface. The onset, which is responsible for the formation of the shock wave in the liquid, is characterized by a high initial velocity of the expanding vapor front ($\approx 1500 \text{ ms}^{-1}$ [30]) .

Fig. 7 a shows a typical stress transient in water for this regime on the lower trace, whereas the upper trace indicates the deflected laser pulse. This stress transient consists of a strong compression pulse followed by a weak negative tail. The total duration of the transient equals that of the laser pulse. The amplitude of the compression reaches several bars at a distance of 2 cm from the impact.

A minimum rise time of 3.6 ns for a pressure difference of 5 bars across the shock front has been recorded for water. Since the shock wave propagates approximately at the sound speed (Section III) , this rise time implies a front thickness L of 5.4 μm . This result is in excellent agreement with the theoretical prediction by Flook and Hornig [58] . They derived an equation for the shock front thickness L in a liquid under isentropic ($S = \text{const}$) conditions:

$$L = \frac{16 \mu C}{3 \cdot \Delta p \cdot \left[1 + \frac{\rho_1}{2C^2} \left(\frac{\partial^2 p}{\partial \rho^2} \right)_S \right]}$$

where μ and C are the shear viscosity and the sound speed of the liquid, respectively.

p indicates the pressure, whereas Δp is the pressure difference across the shock front. ρ is the density, where the subscript 1 refers to the region ahead of the shock front. With the data for water given in [58] , and for $\Delta p = 5$ bar, we obtain from the above equation a shock front thickness $L = 5.3 \text{ } \mu\text{m}$.

The same equation predicts for CCl_4 a shock front at least twice as thick as in water for the same pressure difference across the front. This is in agreement with our observations.

D. Effects for laser energies near the vaporization threshold

In the range, where the absorbed laser-energy density is near the vaporization threshold, two interaction mechanisms are manifested simultaneously: thermoelastic effect and vaporization. A typical stress transient, obtained for H_2O under this condition, is shown in Fig. 7 b . In contrast to the case of dominant vaporization (Fig. 7 a) , the pressure signal consists of two compression pulses, which are separated by a time Δt , that is of the order of magnitude 200 ns .

The prepulse is attributed to the thermoelastic effect.

The following main pulse is due to vaporization.

In Fig. 8 the peak pressures p of the pulses caused by vaporization and by the thermoelastic process are plotted versus the laser peak power P . From these two curves it is obvious that the vaporization process is more effective in transforming electromagnetic power into sound energy.

For the case of vaporization, the peak pressure p is proportional to the laser peak power $(P - P_{th})$, where P_{th} indicates the threshold power related to the vaporization threshold. It should be noticed that P_{th} depends on the focal dimensions and on the transverse mode pattern

(Fig. 5). For the thermoelastic process, no threshold power is expected. However, the measured peak pressure p in Fig. 8 is not proportional to the laser peak power P , but proportional to $(P - P_0)$ for powers $P > P_0$, where P_0 depends on the liquid as is seen in Figs. 8 and 11.

This dependence of the peak pressure p on the laser power P is due to the long tail in the laser pulse. From further investigations, it has been deduced that this tail does not contribute to the sound generation, although it contains part of the laser pulse energy E . This result confirms the transient character of the thermoelastic process.

For an absorbed energy above the vaporization threshold, data on the dependence of the peak pressures on the laser intensity have only been published for laser interaction with solids. Metz et al. [59] , Hettche et al. [60] and Lowder et al. [50] reported that the peak pressure p increases with laser intensity I according to $p \propto I^\gamma$, with $\frac{4}{3} \leq \gamma \leq 2$. The uncertainty in γ is explained qualitatively by different experimental conditions and by plasma formation. Theoretically, a first power dependence within a logarithmic factor is predicted for the case of vaporization at the surface, with no absorption of laser energy in the vapor [50] . Yang [51] , Magee et al. [39] , Fox et al. [61] and Fairand et al. [62] observed peak pressures in solids that are proportional to the incident laser energy, or power density, at laser fluxes that are below the air breakdown threshold. This is in agreement with our results for liquids.

The decrease of the peak pressure p of a spherical wave is expected to be proportional to $1/r$, where r indicates its radius [2, 32] . Our stress measurements confirm this law for both the thermoelastic prepulse and the vaporization pulse. The results obtained for water are presented in Fig. 9 on a double logarithmic diagram.

The peak pressure p for a constant laser peak power P of 60 kW is plotted as a function of r , yielding a slope of -0.98 for the thermoelastic effect, and of -0.96 for the vaporization process. This is in good agreement with the $1/r$ law, which is also found for the stress wave in *n*-heptane.

Nevertheless, it should be pointed out that the $1/r$ law is valid only for small pressure amplitudes. For high amplitudes both the thermal conduction and the viscosity of the liquid, become important [63]. Therefore, only a lower limit of the peak stress near the laser impact can be derived from the $1/r$ law. If a transient with a peak pressure of 5 bars at $r = 4$ cm originates from a laser impact with a radius of $r_0 = 0.2$ mm, the peak pressure near the impact is at least 1 kbar. This demonstrates, that, even for modest laser intensities, high-pressure transients are generated in absorbing liquids.

The time interval Δt between the thermoelastic prepulse and the vaporization pulse shown in Fig. 7 b represents the delay between the laser impact and the onset of vaporization.

Under our experimental conditions this time interval Δt is independent on the distance r from the impact. Near the impact the speed of the strong shock wave caused by vaporization is higher than that of the weak shock wave caused by the thermoelastic process. At some distance from the impact both shock waves propagate at the same speed, namely the sound speed. Therefore at measuring distances the time interval remains constant. In the case of dominant vaporization (Section V C) the thermoelastic prepulse is overtaken and suppressed by the strong vaporization shock wave.

The time interval Δt decreases with increasing peak amplitude of the vaporization pulse, hence with increasing laser peak power P . We found the relation

$$\Delta t = \text{const} \cdot P^{-\eta}$$

according to Fig. 10, where $\log \Delta t$ is plotted versus $\log P$ for water and n-heptane. This plot yields $\eta = 0.76$ for water and $\eta = 0.54$ for n-heptane. The above equation is in accordance with the fact, that for our and other lasers, a high peak power P corresponds to a fast rise time. Thus, the vaporization threshold is reached earlier. Consequently Δt is reduced.

We found, that the ratio of the time interval Δt to the rise time of the laser pulse is approximately 1 for water, and 3.2 for n-heptane. The higher ratio of n-heptane is related to the larger absorbing volume in n-heptane, which has the lower absorptivity. Hence the vaporization threshold is reached later.

Our experimental results of stress generation in liquids near the vaporization threshold are in good agreement with the theoretical one-dimensional model of Feiock and Goodwin [64] for laser-induced stresses in water. They used a hydrodynamic computer code which incorporates the thermal conductivity and the equation of state that includes vaporization. This is the only model taking a phase change into account. It predicts a stress transient consisting of a prepulse associated with the thermoelastic process and a delayed vaporization pulse.

In the case of strong vaporization, the model predicts the overtaking of the prepulse by the vaporization pulse, which is also in agreement with our experiments. The authors call attention to the fact, that the vaporization process is more efficient than the thermoelastic mechanism. The efficiencies of the two processes depend on the properties of the liquids. In general they are below 1 % [3, 18, 64] .

E. Effects for laser energies below the vaporization threshold

If the laser energy density is insufficient for the vaporization, the thermoelastic process alone is responsible for the generation of acoustic waves. For a laser impact on the free surface of a liquid this process gives rise to a rarefaction wave following the compression wave. As mentioned in Chapter III , rarefaction may cause cavitation. Before discussing the time dependence of the acoustic wave in detail, we should mention an important phenomenon, which can occur at laser energies below the vaporization threshold.

As mentioned in Section V A , vaporization of CCl_4 requires higher laser energies than vaporization of water or n-heptane, because of the low absorptivity of CCl_4 . Thus, the pure thermoelastic process can be studied in CCl_4 at higher laser powers than in water or n-heptane. In the course of our studies on laser-induced acoustic waves in CCl_4 , we discovered a saturation of the peak pressure p with increasing laser power P . This saturation was observed neither in water, nor in n-heptane, since these liquids vaporize already at lower laser energies. Fig.11 illustrates the pressure saturation in CCl_4 for both the hemi-spherical and the cylindrical acoustic waves in comparison with n-heptane.

For CCl_4 the relation between p and P is not linear as for n-heptane and for water (Fig. 8) in the thermoelastic regime. In CCl_4 , the pressure saturates for both waves at a laser power P_{sat} of approximately 100 kW .

This phenomenon, which is observed for the first time in a liquid, differs from saturation effects of the peak stress induced in solids. These were reported by Magee et al. [39] and Fox et al. [61] . They attributed the pressure saturation in solids to the shielding of the target surface by the formation of a dense surface plasma at high laser intensities. Yet in our experiment neither plasma formation nor vaporization are responsible, because both are absent. Since pressure saturation occurs for the hemi-spherical and the cylindrical acoustic waves in CCl_4 , a reduced absorptivity of the laser radiation at higher powers has to be taken into account. A reduced absorption was already manifested in the shadowgraphs discussed in Chapter III . Hence we introduce an absorption coefficient α , which depends on the laser peak power P .

Since the laser intensity I in the focus is proportional to the peak power P , we choose $\alpha(P)$ in accordance with the absorption characteristics of saturable dyes, as reported by Bushanam [63]. For the case of homogeneous broadening, which is expected in our experiment, we may write

$$\alpha(P) = \alpha_0 \cdot \frac{P_{\text{sat}}}{P_{\text{sat}} + P},$$

where α_0 and P_{sat} indicate the low-power limit of $\alpha(P)$ and the saturation power, respectively. For water and n-heptane, we have found $p \propto P - P_0$ for $P > P_0$. Since α is constant for these liquids, the induced peak pressure p is proportional to the absorbed power: $p \propto \alpha \cdot (P - P_0)$. This relation should also be valid for CCl_4 with $\alpha = \alpha(P - P_0)$. Therefore

$$p \propto \frac{(P - P_0)}{(P - P_0) + P_{\text{sat}}} \quad \text{with } P > P_0.$$

With $P_{\text{sat}} = 100$ kW and $P_0 = 0$ kW for the cylindrical wave, and $P_0 = 20$ kW for the hemi-spherical wave in accordance with Fig. 11, this function is plotted for both waves in Figs. 12 a and 12 b.

The two plots confirm the linearity with coefficients r^2 for the regression lines which are 0.95 for the cylindrical wave, and 0.98 for the hemi-spherical wave. Therefore, the reduced absorptivity of CCl_4 at higher laser powers is justified.

In water, the pure thermoelastic process is obtained only by defocusing the laser beam. A typical acoustic signal for this case is presented in Fig. 7 c on the lower trace. Two events are recorded for two subsequent laser pulses. The almost complete overlapping of the signals demonstrates the excellent reproducibility. In contrast to the recordings obtained for the laser energy densities well above (Fig. 7 a) and near (Fig. 7 b) the vaporization threshold, this signal consists of a compression followed by an almost symmetric rarefaction. At approximately 300 ns after the positive peak pressure, the amplitude of the pressure pulse, as seen in Fig. 7 c, becomes positive, which reflects the onset of very slight vaporization. The total duration of the acoustic signal is equal to the duration of the laser pulse.

Hitherto, no experimental data has been published on the time dependence of a thermoelastic acoustic wave, generated by the transient heating of an absorbing liquid by the impact of a CO_2 laser pulse.

Theoretical models for thermoelastic stress wave generation, without the inclusion of a phase change, have been proposed by several authors, yet only Hu [2] presented a three dimensional theory with an analytical treatment of thermoelastic spherical waves. The model yields a symmetric pressure signal with respect to the time axis, peak amplitudes proportional to the laser power P , and inversely proportional to the radius r .

The symmetry with respect to the time axis, as well as the $1/r$ law, have been verified by our experiment.

Whereas the calculated peak pressures are within an order of magnitude of the measured values, the theoretical time dependence, though symmetrical, deviates considerably from the experiment. This is demonstrated in Fig. 13, where the acoustic signal according to Hu is superimposed on the experimental record for water, shown in Fig. 7c. For this purpose the peak amplitudes were normalized.

Not only the temporal shapes of the compressive and the rarefaction wave, but also their time separation T does not coincide between theory and experiment.

In the model of Hu, T is given by the duration t_L of the laser pulse. Therefore T should be independent of the properties of the liquid. However, the measured values for T are 160 ns for water, 470 ns for n-heptane, and 750 ns for CCl_4 for a constant laser pulse duration t_L of approximately 350 ns. In view of these discrepancies we have developed a new theory which yields considerably better agreement with the experiment. This analytical model is presented in Part II.

VI. CONCLUSIONS

Shadowgraphy in conjunction with measurements that employ especially developed stress transducers, have been demonstrated as suitable for the study of laser-generated stress waves in liquids. The experiments show the drastic influence of the spatial and temporal characteristic of the laser pulse on the stress generation. An important result of these investigations are the generation and detection of high-frequency sound waves with tunable frequency. Furthermore we were able to examine the individual influences of the thermoelastic effect, and of the vaporization process, on the time dependence and the value of the peak amplitude of the induced stress transient. These two processes are the dominant interaction mechanisms for the laser energies and the liquids employed in this study. Thermoelastic pressure pulses in CCl_4 have shown a saturation in the peak pressure with increasing laser pulse power. This phenomenon has been interpreted successfully by the assumption of a reduced absorption of CCl_4 at higher incident power. The agreement between our measured time dependence of the thermoelastic wave, and the calculated time dependence, according to the three-dimensional model of Hu, is insufficient. Therefore, a new model has been developed which is presented in Part II .

REFERENCES

1. G.A. Askar'yan, A.M. Prokhorov,
G.F. Chanturiya and G.P. Shipulo,
Sov. Phys. JETP 17, 1463 (1963)
2. C.L. Hu,
J. Acoust. Soc. Am. 46, 728 (1969)
3. R.M. White,
J. Appl. Phys. 34, 3559 (1963)
4. P.A. Barnes, Ph.D. thesis
(Simon Fraser University, 1969)
5. C.E. Bell and J.A. Landt,
Appl. Phys. Lett. 10, 46 (1967)
6. M.P. Felix and A.T. Ellis,
Appl. Phys. Lett. 19, 484 (1971)
7. E.F. Carome, E.M. Carreira and C.J. Prochaska,
Appl. Phys. Lett. 11, 64 (1967)
8. J.J. Condon
(John Carroll University, 1973, unpublished)
9. E.F. Carome, C.E. Moeller and N.A. Clark,
J. Acoust. Soc. Am. 40, 1462 (1966)
10. R.G. Brewer and K.E. Rieckhoff,
Phys. Rev. Lett. 13, 334 (1964)

11. R.Y. Chiao, C.H. Townes and B.P. Stoicheff,
Phys. Rev. Lett. 12, 592 (1964)
12. F.V. Bunkin, N.V. Karlov, V.M. Komissarov
and G.P. Kuz'min,
JETP Lett. 13, 341 (1971)
13. N.N. Botygina, V.I. Bukatyi and
S.S. Khmelevtsov,
Sov. Phys. Acoust. 22, 368 (1976)
14. S.F. Cleary and P.E. Hamrick,
J. Acoust. Soc. Am. 46, 1037 (1969)
15. C.E. Bell and B.S. Maccabee,
Appl. Optics 13, 605 (1974)
16. M. Sigrist and F. Kneubühl,
ZAMP 27, 517 (1976)
17. E.F. Carome, N.A. Clark and C.E. Moeller,
Appl. Phys. Lett. 4, 95 (1964)
18. L.S. Gournay,
J. Acoust. Soc. Am. 40, 1322 (1966)
19. M. Sigrist, B. Adam and F. Kneubühl,
Phys. Lett. 42A, 352 (1973)
20. M. Sigrist and F.K. Kneubühl,
Appl. Phys. 2, 43 (1973)

21. N. Bloembergen,
IEEE J. Quantum Electron. QE-10, 375 (1974)
22. A. Gondhalekar, E. Holzhauer and
N.R. Heckenberg,
Phys. Lett. 46A, 229 (1973)
23. A. Girard,
Opt. Comm. 11, 346 (1974)
24. A.K. Levine, Ed., Lasers
(Marcel Dekker, Inc., New York 1968), Vol. II .
25. D.C. Emmony, M. Sigrist and F.K. Kneubühl,
Appl. Phys. Lett. 29, 547 (1976)
26. W. Lauterborn,
Appl. Phys. Lett. 21, 27 (1972)
27. J. Beinert, private communication
28. H.D. Downing and D. Williams,
J. Geophys. Res. 80, 1656 (1975)
29. P.R. Langaker and M.M. Litvak,
J. Appl. Phys. 40, 4033 (1969)
30. D.C. Emmony, B.M. Geerken and A. Straaijer,
Infrared Phys. 16, 87 (1976)

31. L.D. Rozenberg, Ed., High-Intensity Ultrasonic Fields (Plenum Press, New York and London, 1971)
32. R.H. Cole, Underwater Explosions (Princeton U.P., Princeton, 1948)
33. M.A. Cook, R.T. Keyes and W.O. Ursenbach, J. Appl. Phys. 33, 3413 (1962)
34. W.J. Halpin, O.E. Jones and R.A. Graham, in Symposium on Dynamic Behavior of Material, ASTM Special Technical Publication No. 336 (ASTM, Philadelphia, Pa., 1963)
35. R.A. Graham, F.W. Neilson and W.B. Benedick, J. Appl. Phys. 36, 1775 (1965)
36. R.A. Graham and R.D. Jacobson, Appl. Phys. Lett. 23, 584 (1973)
37. R.A. Graham, J. Appl. Phys. 46, 1901 (1975)
38. J.C. Bushnell and D.J. Mc Closkey, J. Appl. Phys. 39, 5541 (1968)
39. T.J. Magee, R.A. Armistead and P. Krehl, J. Phys. D : Appl. Phys. 8, 498 (1975)
40. N.C. Anderholm, Appl. Phys. Lett. 16, 113 (1970)

41. N.C. Anderholm and R.R. Boade,
J. Appl. Phys. 43, 434 (1972)
42. P.S. Peercy, E.D. Jones, J.C. Bushnell
and G.W. Gobeli,
Appl. Phys. Lett. 16, 120 (1970)
43. M.P. Felix and A.T. Ellis,
Appl. Phys. Lett. 21, 532 (1972)
44. M.P. Felix,
Rev. Sci. Instrum. 45, 1106 (1974)
45. J.D. O'Keefe and C.H. Skeen,
Appl. Phys. Lett. 21, 464 (1972)
46. J.A. Fox,
Appl. Phys. Lett. 24, 461 (1974)
47. J.A. Fox,
Appl. Optics 13, 1760 (1974)
48. P. Krehl, F. Schwirzke and A.W. Cooper,
J. Appl. Phys. 46, 4400 (1975)
49. R.M. White,
J. Appl. Phys. 34, 2123 (1963)
50. J.E. Lowder and L.C. Pettingill,
Appl. Phys. Lett. 24, 204 (1974)

51. L.C. Yang,
J. Appl. Phys. 45, 2601 (1974)
52. C.F. Huff and R.A. Graham,
Appl. Phys. Lett. 27, 163 (1975)
53. F.J. Meyer, Ph.D. thesis
(Technische Hochschule Aachen, 1972)
54. L. Bergmann, Der Ultraschall
(S. Hirzel Verlag Stuttgart, 1954)
55. K.F. Herzfeld and T.A. Litovitz,
Absorption and Dispersion of Ultrasonic Waves
(Academic Press, New York and London, 1959)
56. M.J. Brienza and A.J. de Maria,
Appl. Phys. Lett. 11, 44 (1967)
57. R.J. von Gutfeld and R.L. Melcher,
Appl. Phys. Lett. 30, 257 (1977)
58. W.M. Flook and D.F. Hornig,
J. Chem Phys. 23, 816 (1955)
59. S.A. Metz, L.R. Hettche, R.L. Stegman
and J.T. Schriempf,
J. Appl. Phys. 46, 1634 (1975)
60. L.R. Hettche, J.T. Schriempf and R.L. Stegman,
J. Appl. Phys. 44, 4079 (1973)

61. J.A. Fox and D.N. Barr,
Appl. Optics 12, 2547 (1973)
62. B.P. Fairand and A.H. Clauer,
Optics Comm. 18, 588 (1976)
63. G.S. Bushanam and F.S. Barnes,
J. Appl. Phys. 46, 2074 (1975)
64. F.D. Feiock and L.K. Goodwin,
J. Appl. Phys. 43, 5061 (1972)

TABLE I

Absorption coefficients α of various liquids at 10.6 μm
wavelength.

| liquid | $\alpha [\text{cm}^{-1}]$ |
|---|---------------------------|
| water | 870 |
| 1,2-dichlorethane | 322 |
| liquid paraffin | 64 |
| n-heptane | 29 |
| benzene | 21 |
| n-hexane | 13 |
| N, N-dimethylformamide | 11 |
| chloroform | 9 |
| carbon tetrachloride (CCl_4) | 5 |
| n-pentane | 3 |
| carbon disulfide (CS_2) | <1 |

TABLE II

Physical Properties of Liquids Investigated

| | Water | CCl ₄ | n-heptane |
|--|-----------------------|------------------------|------------------------|
| density ρ [kg m ⁻³] | 10 ³ | 1.59·10 ³ | 0.68·10 ³ |
| specific heat σ [J kg ⁻¹ deg ⁻¹] | 4.19·10 ³ | 0.84·10 ³ | 2.26·10 ³ |
| heat of vaporization [J kg ⁻¹] | 2.26·10 ⁶ | 0.21·10 ⁶ | 0.35·10 ⁶ |
| vaporization threshold [J m ⁻³] | 2.6 ·10 ⁹ | 0.41·10 ⁹ | 0.36·10 ⁹ |
| cubic thermal expansion coefficient β [deg ⁻¹] | 18 ·10 ⁻⁵ | 122 ·10 ⁻⁵ | 124.4·10 ⁻⁵ |
| sound velocity C [m s ⁻¹] | 1.49·10 ³ | 0.94·10 ³ | 1.16·10 ³ |
| absorption coefficient α at 10.6 μ m [cm ⁻¹] | 870 | 5 | 29 |
| sound attenuation coefficient δ/f^2 (f = sound frequency) [s ² cm ⁻¹] | 25 ·10 ⁻¹⁷ | 530 ·10 ⁻¹⁷ | 80 ·10 ⁻¹⁷ |

FIGURE CAPTIONS

- Fig. 1 Two different transverse mode patterns, corresponding to adjacent P transitions, near the focus of the laser beam.
- Fig. 2 a Hemi-spherical shock wave in water. The picture was taken $1.8 \mu\text{s}$ after the laser impact with an exposure time of 200 ns.
- Fig. 2 b Hemi-spherical and cylindrical shock wave in n-pentane, photographed $3.5 \mu\text{s}$ after the laser impact. The horizontal bars are spaced by 2 mm and the exposure time is 200 ns .
- Fig. 2 c Laser-induced breakdown and subsequent formation of spherical shock waves in CS_2 .
- Fig. 3 Schematic diagram of the stress transducer.
- Fig. 4 Experimental arrangement for stress measurements with the aid of a transducer.

Fig. 5 Peak pressures in water for two different transverse modes of the hybrid CO₂ laser as a function of the incident laser peak power at a constant distance from the impact.

Fig. 6 Upper trace: self mode-locked laser pulse
 (time 50 ns/div)

 Lower trace: Corresponding thermoelastic
 40 MHz acoustic wave in water
 (time 50 ns/div)

Fig. 7 a Upper trace: Pulse of the hybrid CO₂ laser.
Lower trace: Stress transient in water for
laser pulse energies well above
the vaporization threshold.

Fig. 7 b Upper trace: Pulse of the hybrid CO₂ laser.
Lower trace: Stress transient in water for
laser pulse energies near the
vaporization threshold.

- Fig. 7 c Upper trace: Pulse of the hybrid CO_2 laser
Lower trace: Stress transient in water for
laser pulse energies below the
vaporization threshold.
- Fig. 8 Peak pressures p in water as a function of
the laser peak power P for the vaporization
process and for the thermoelastic effect at
a constant distance r from the impact.
- Fig. 9 Peak pressures in water as a function of the
distance r from the impact for both, the
vaporization process and the thermoelastic
effect. The peak power of the laser pulses
is 60 kW. (Double logarithmic scale).
- Fig. 10 Time interval Δt between the thermoelastic
prepulse and the vaporization pulse as a
function of the laser peak power P for water
and n-heptane at a constant distance r from
the impact. (Double logarithmic scale).

Fig. 11 Pressure saturation for the cylindrical and the hemi-spherical wave in CCl_4 , in comparison to the hemi-spherical wave in n-heptane.

Fig. 12 a Peak pressure for the hemi-spherical wave in CCl_4 as a function of the normalized peak power, which represents the power-dependent absorptivity $\alpha(P-P_0)$.

Fig. 12 b Peak pressure for the cylindrical wave in CCl_4 as a function of the normalized peak power, which represents the power-dependent absorptivity $\alpha(P)$.

Fig. 13 Theoretical thermoelastic acoustic wave according to Hu (dashed curve) superimposed on the experimental record (solid curve).

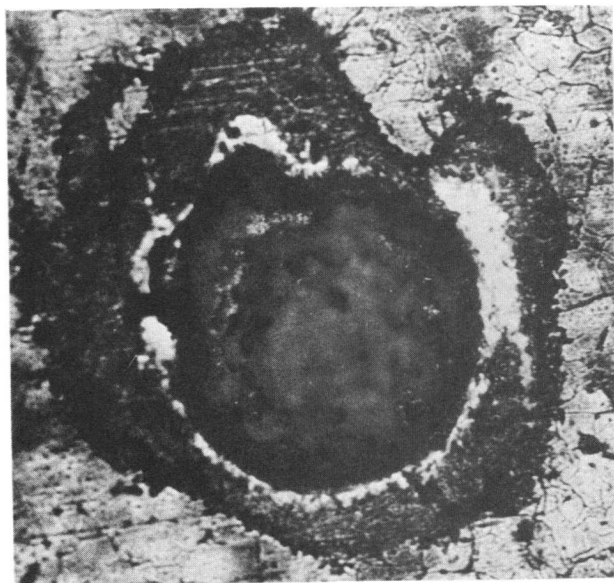
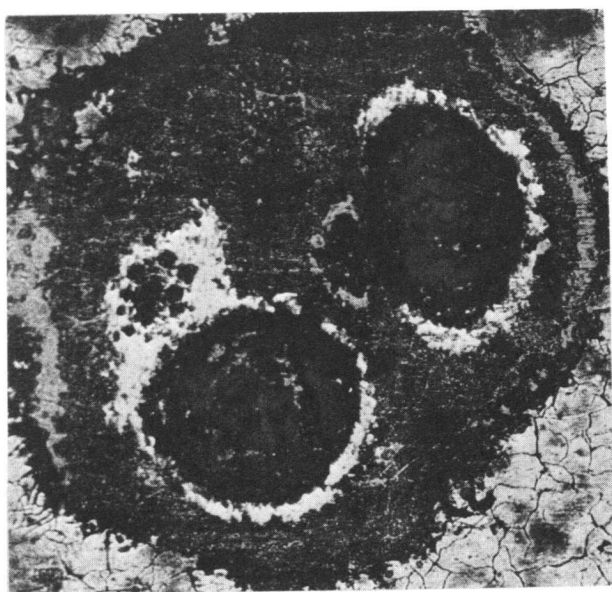


Fig. 1

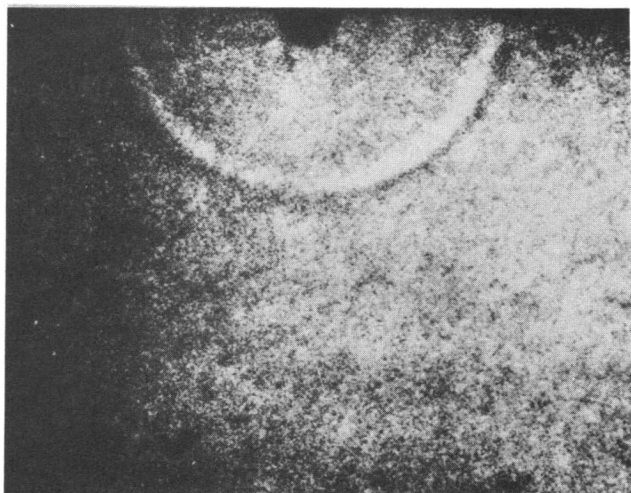


Fig. 2a

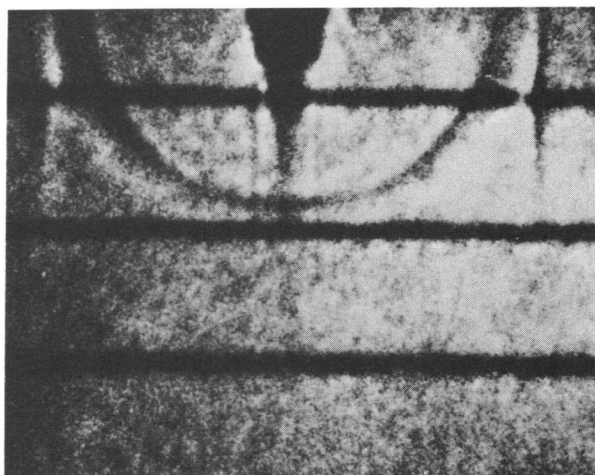


Fig. 2b

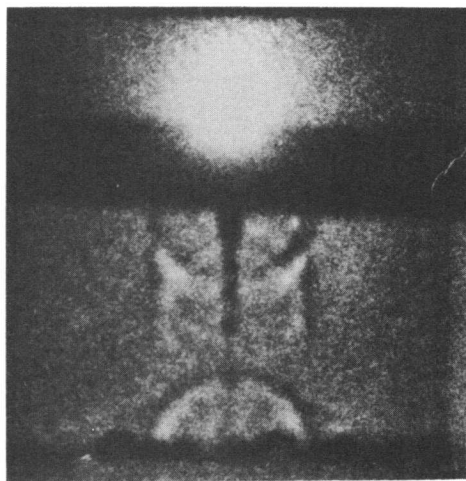


Fig. 2c

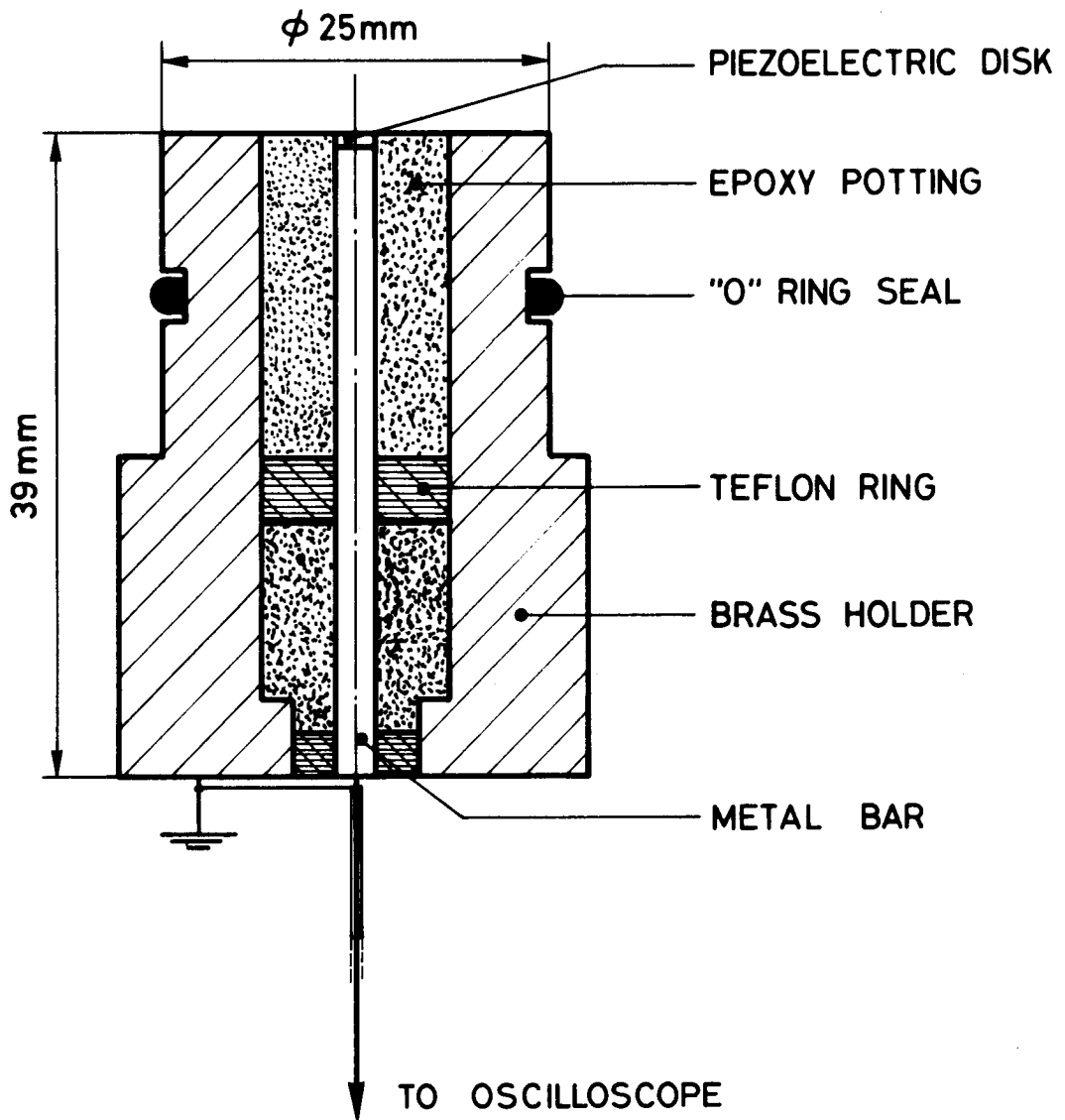


Fig. 3

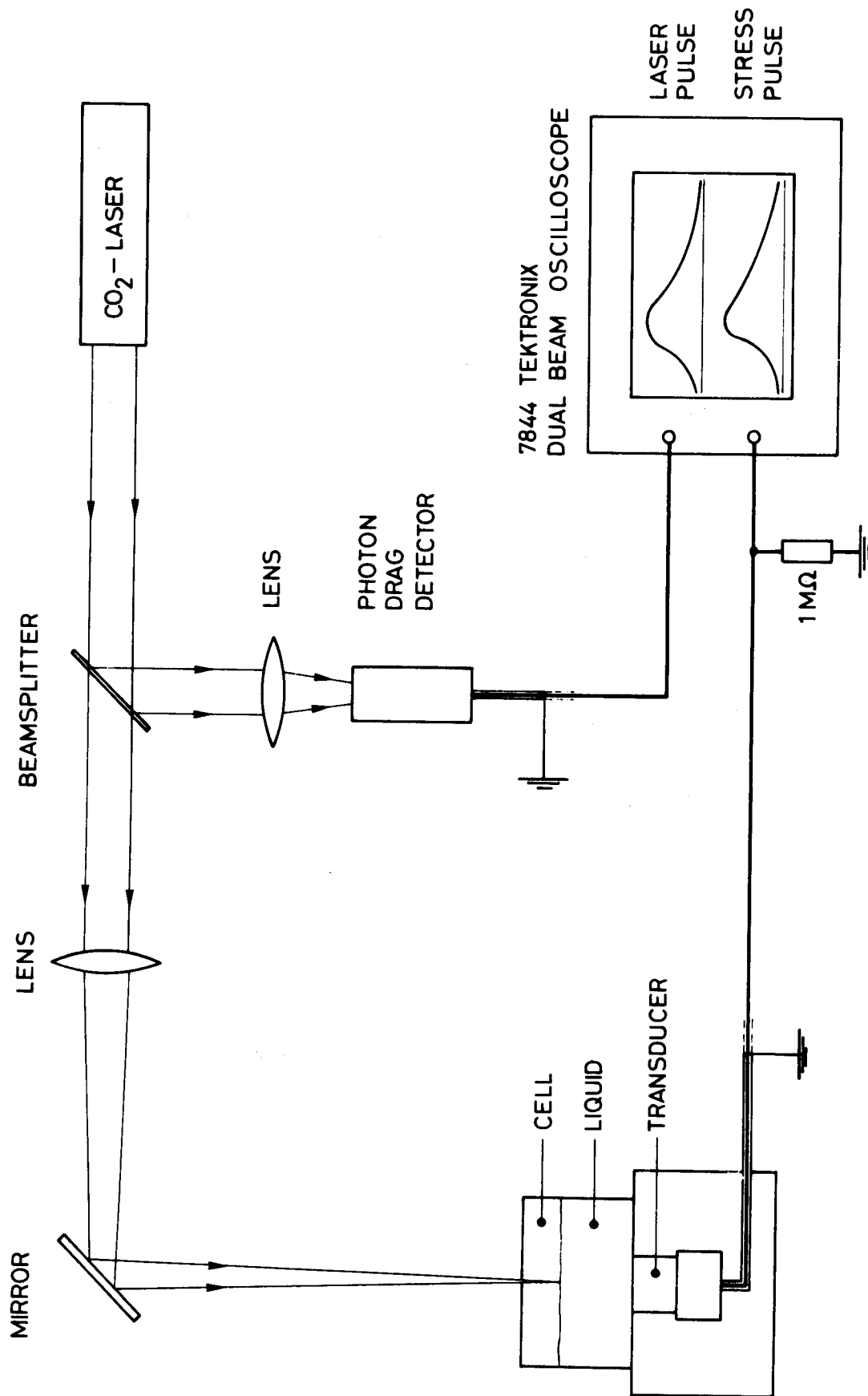


Fig. 4

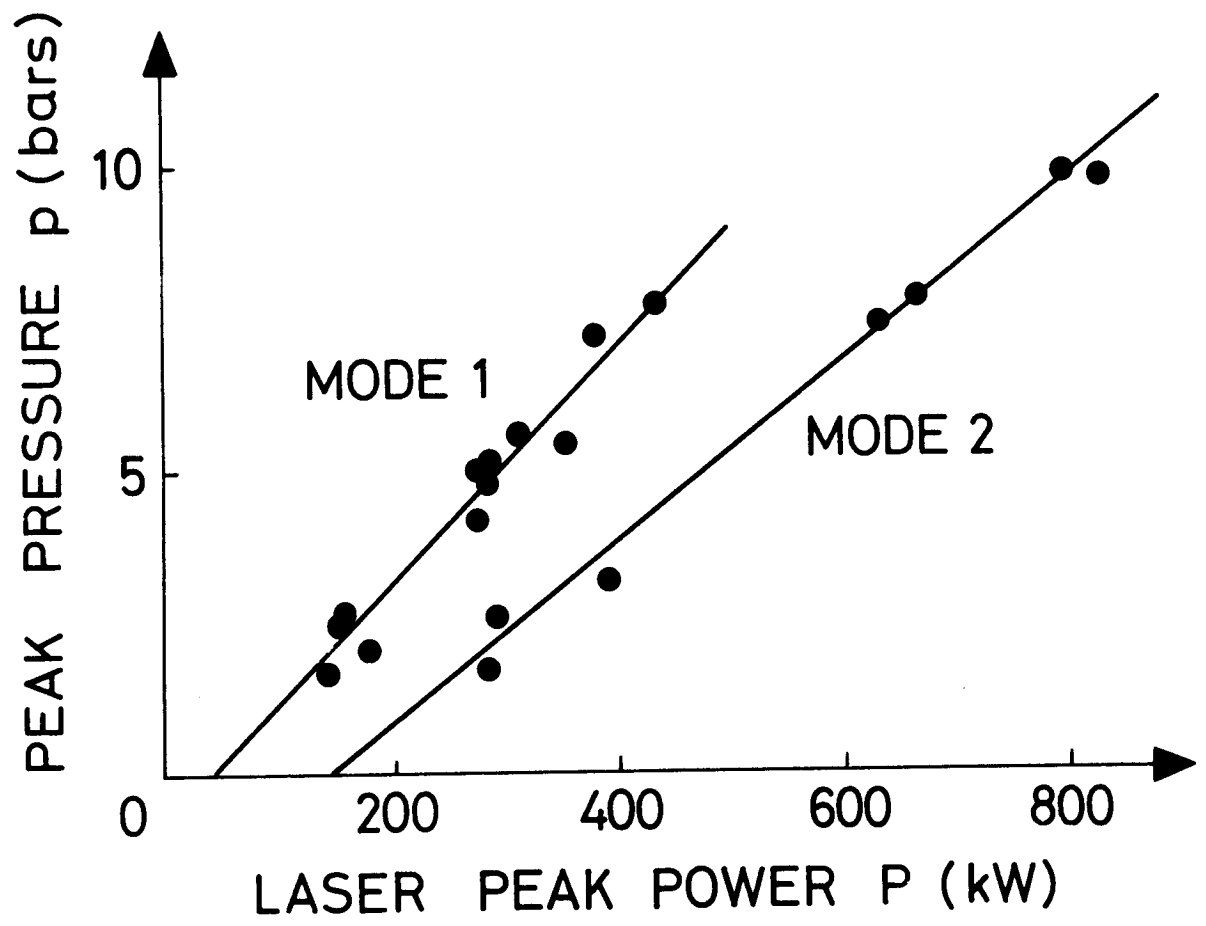


Fig. 5

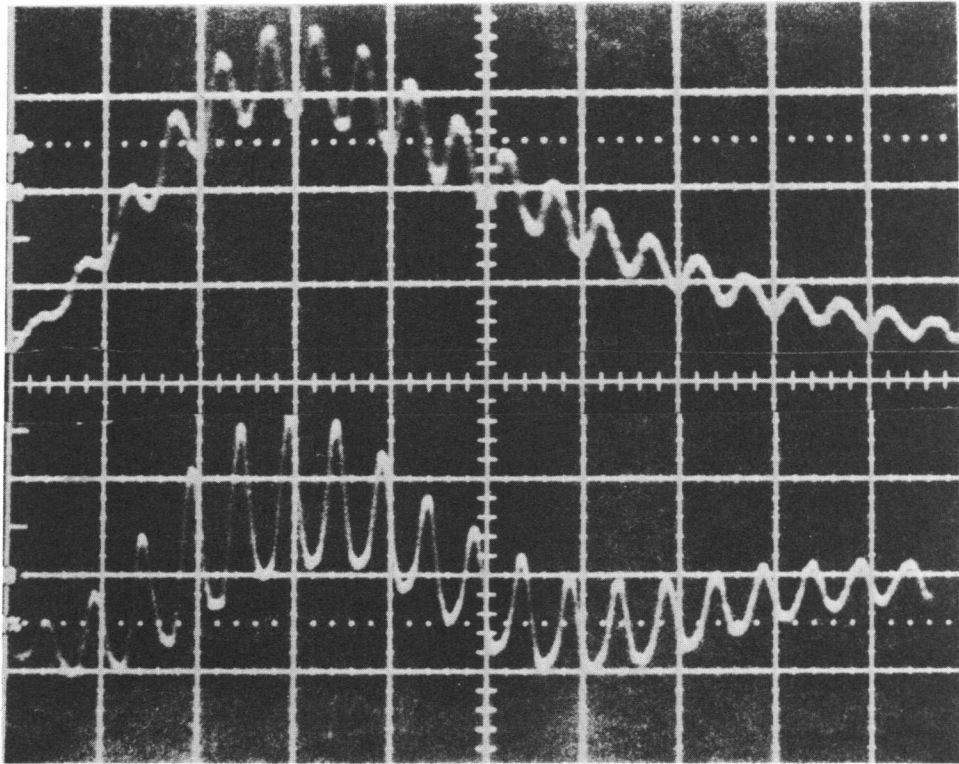


Fig. 6

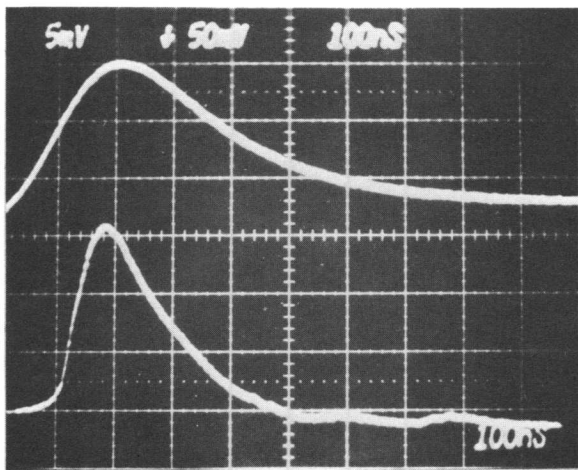


Fig. 7a

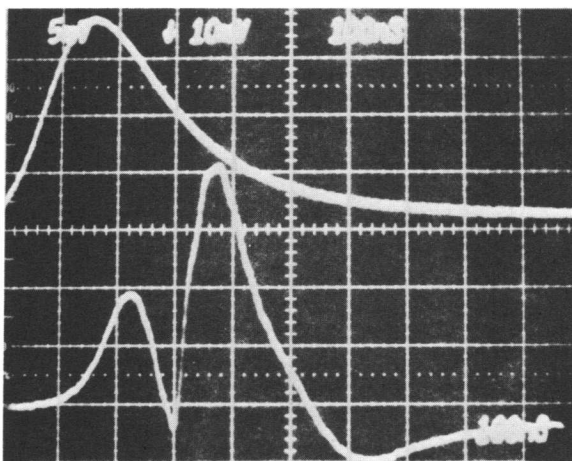


Fig. 7b

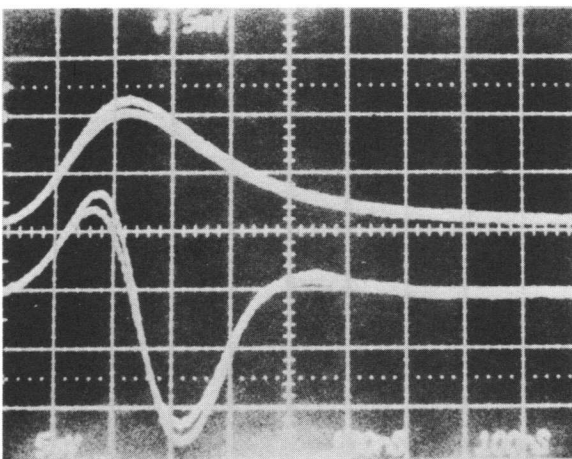


Fig. 7c

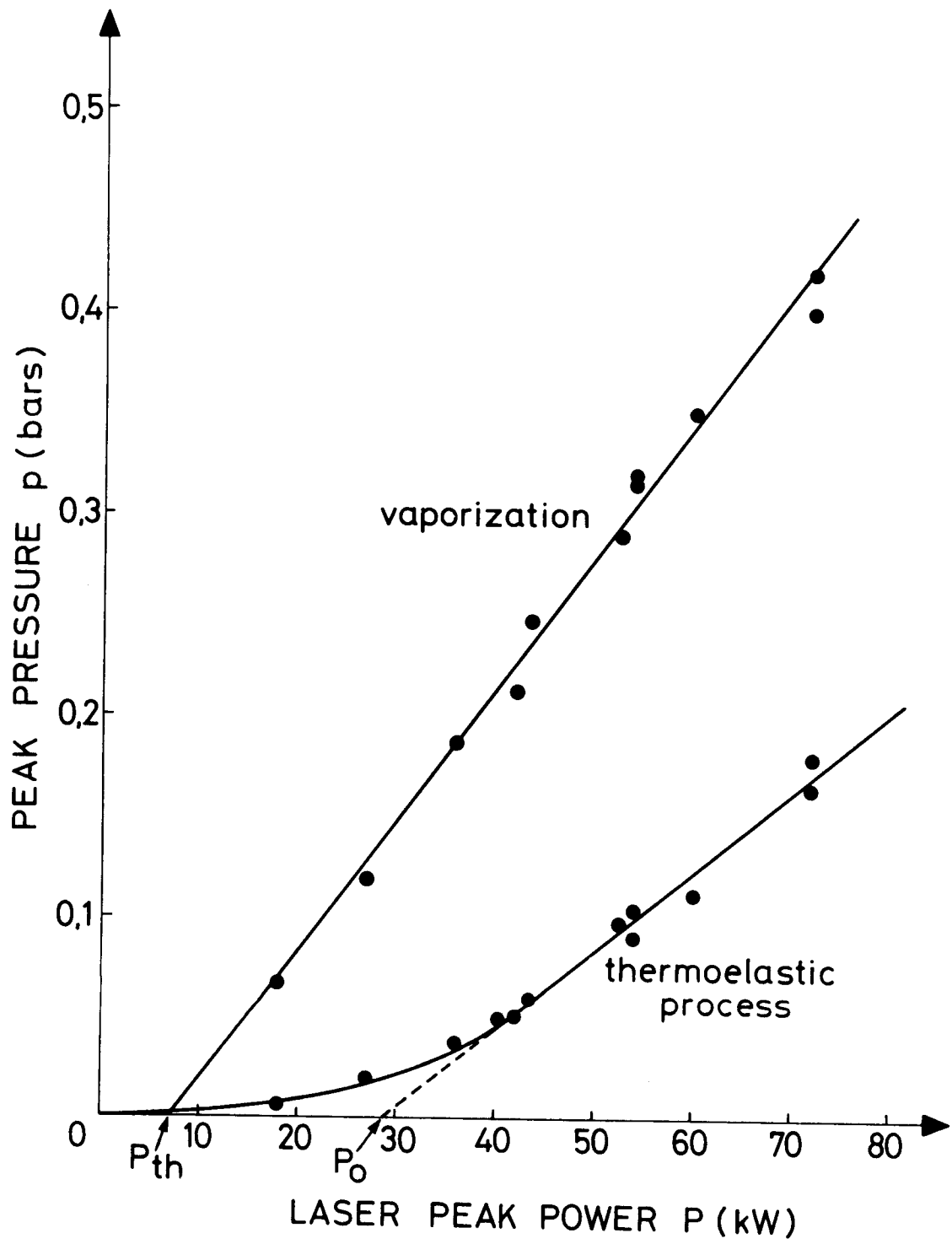


Fig. 8

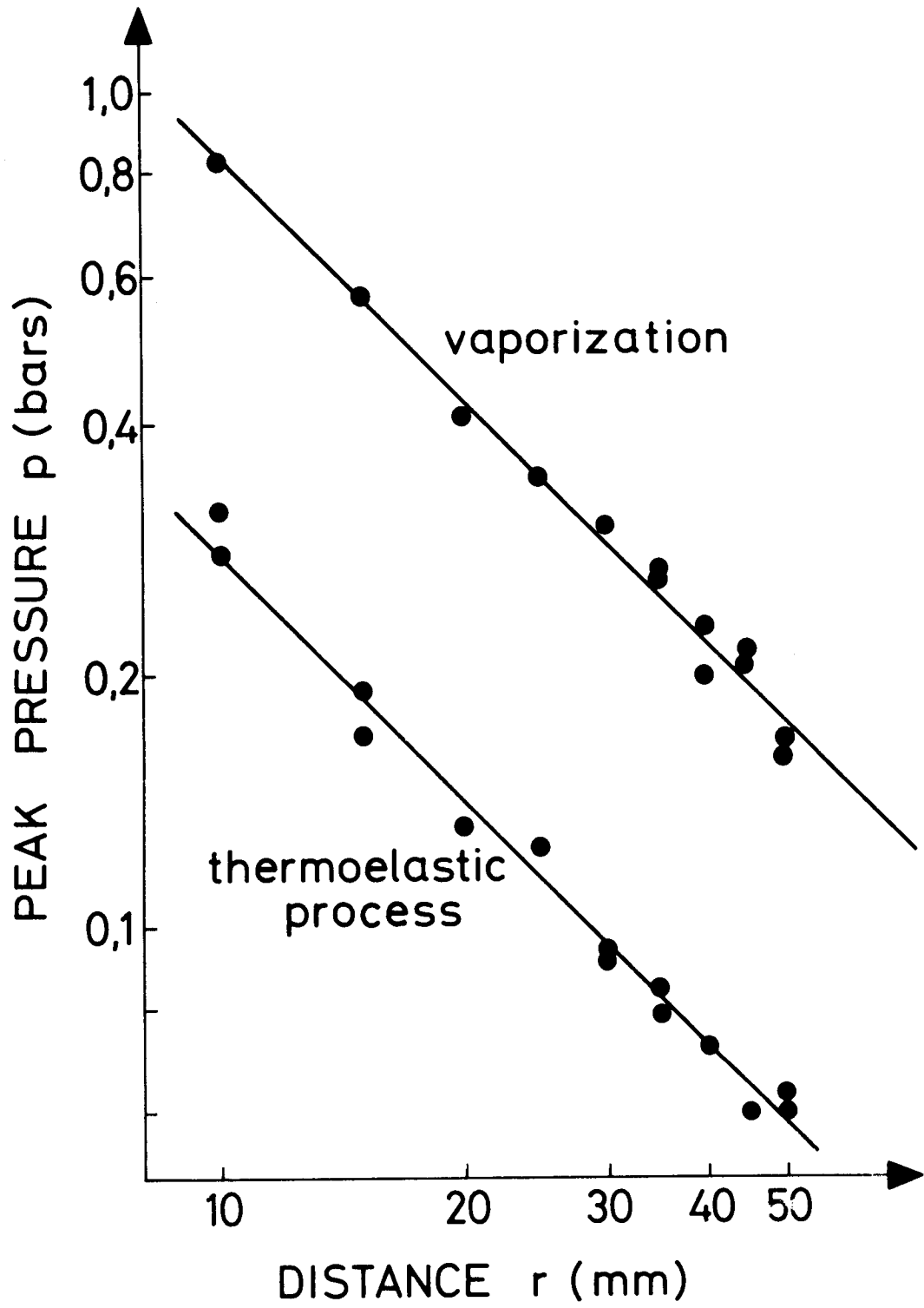


Fig. 9

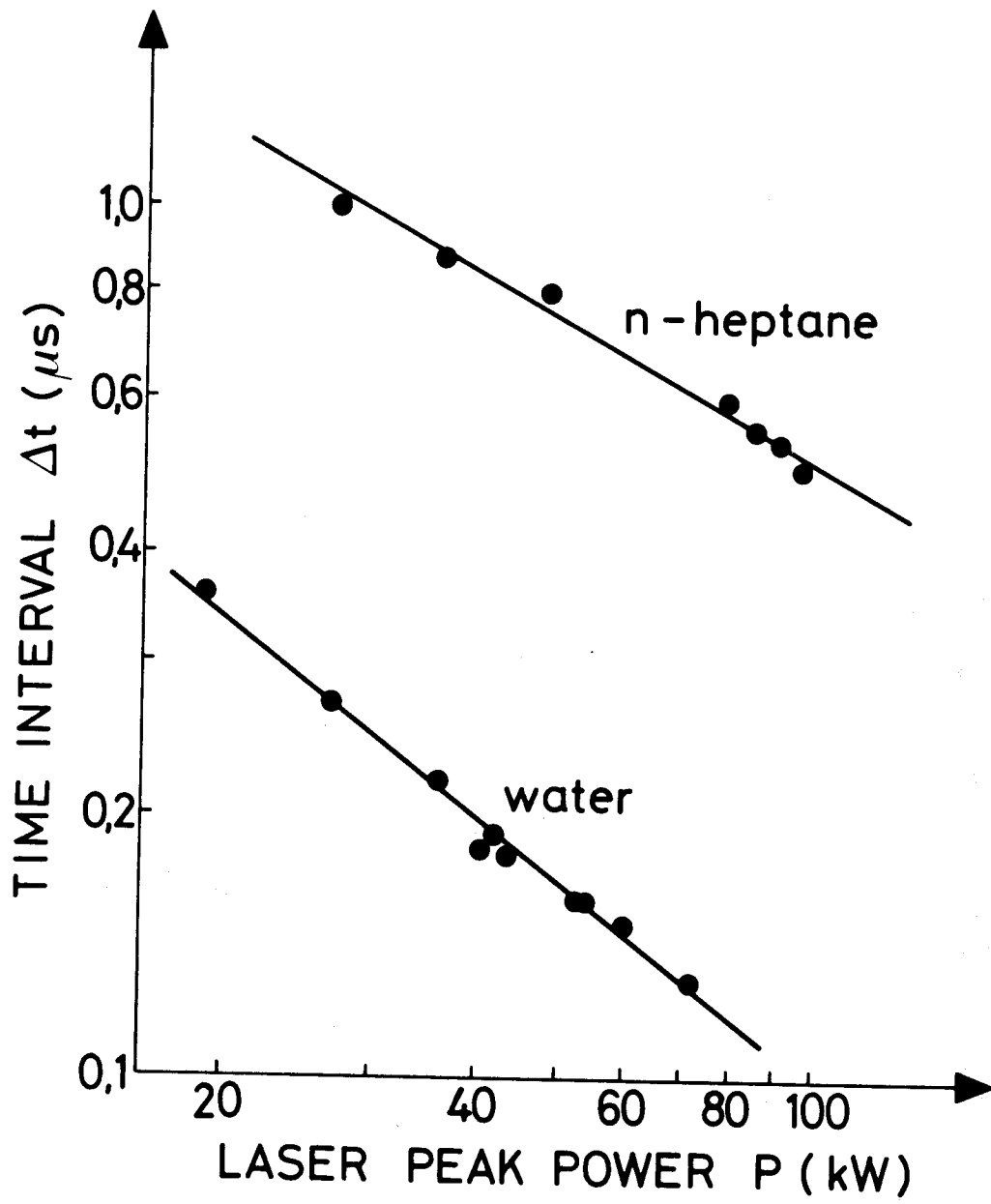


Fig. 10

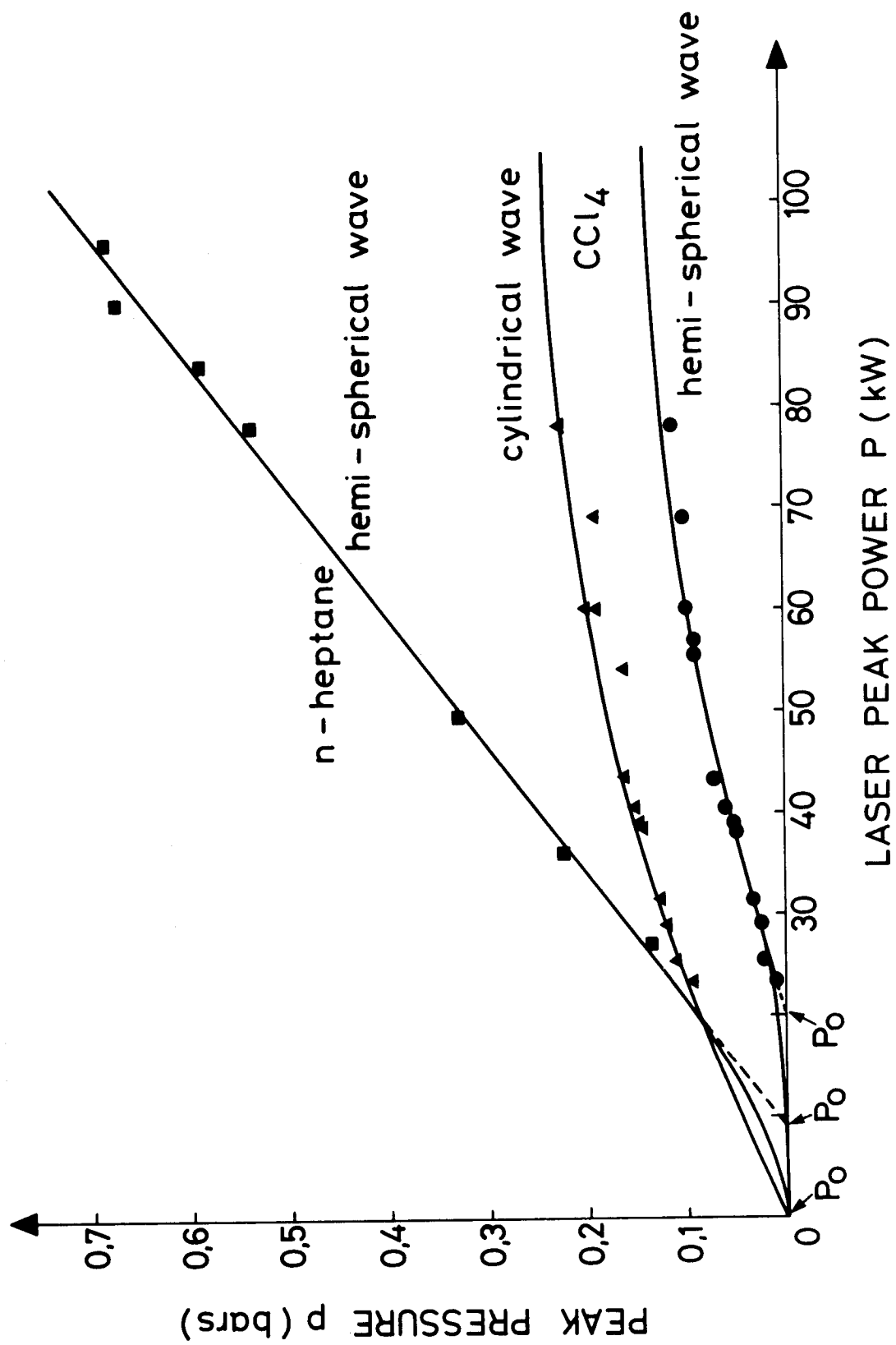


Fig. 11

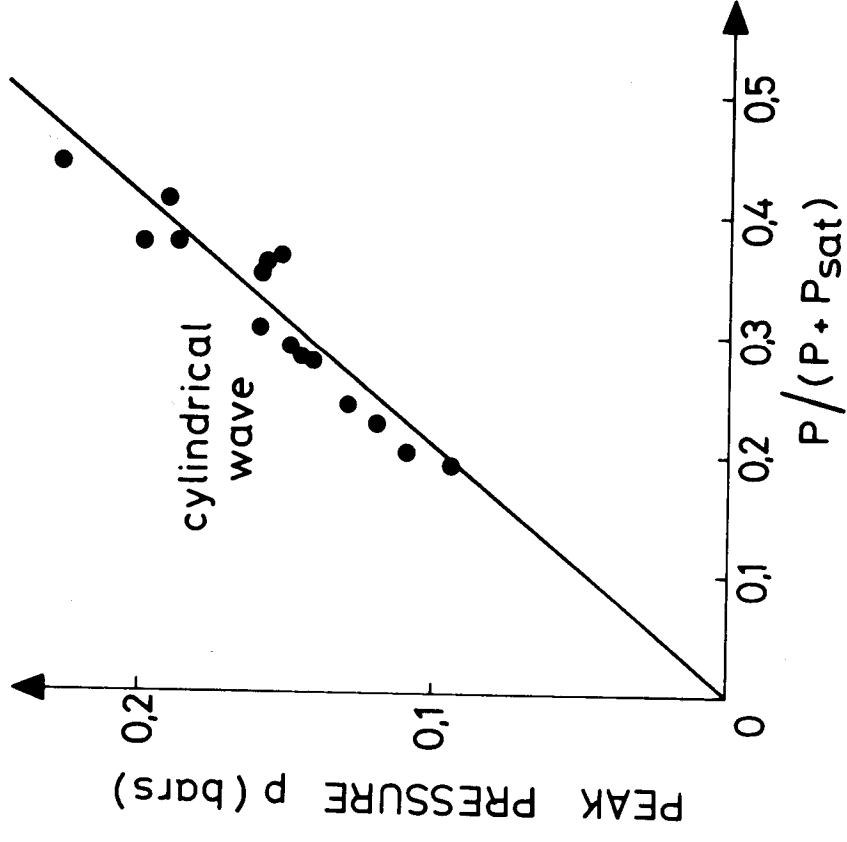


Fig.12 b

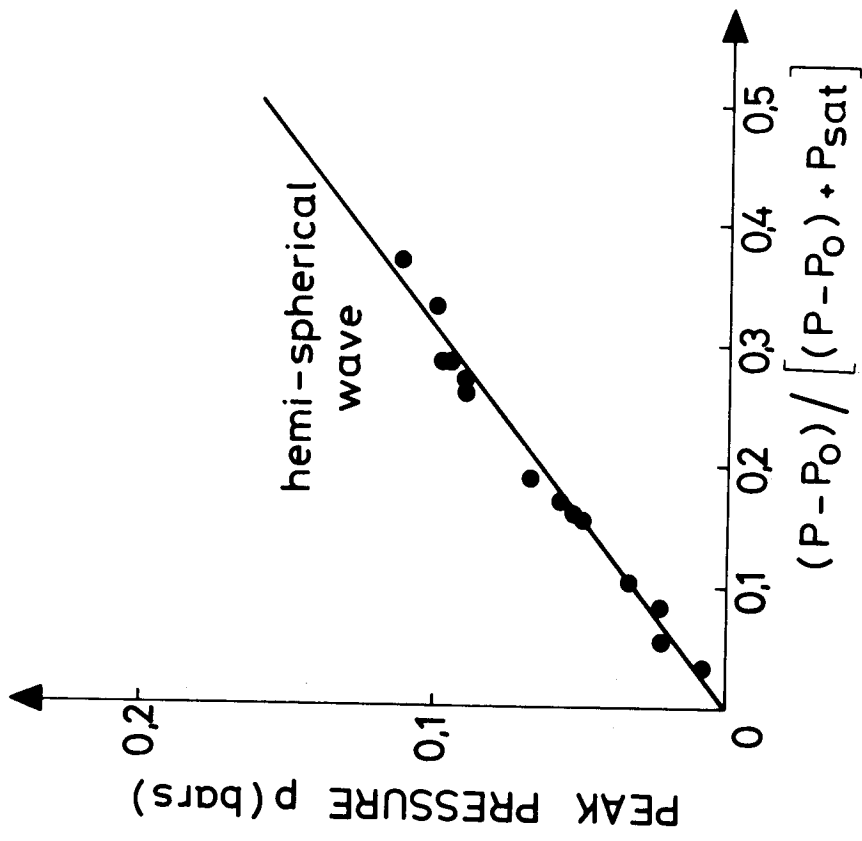


Fig.12 a

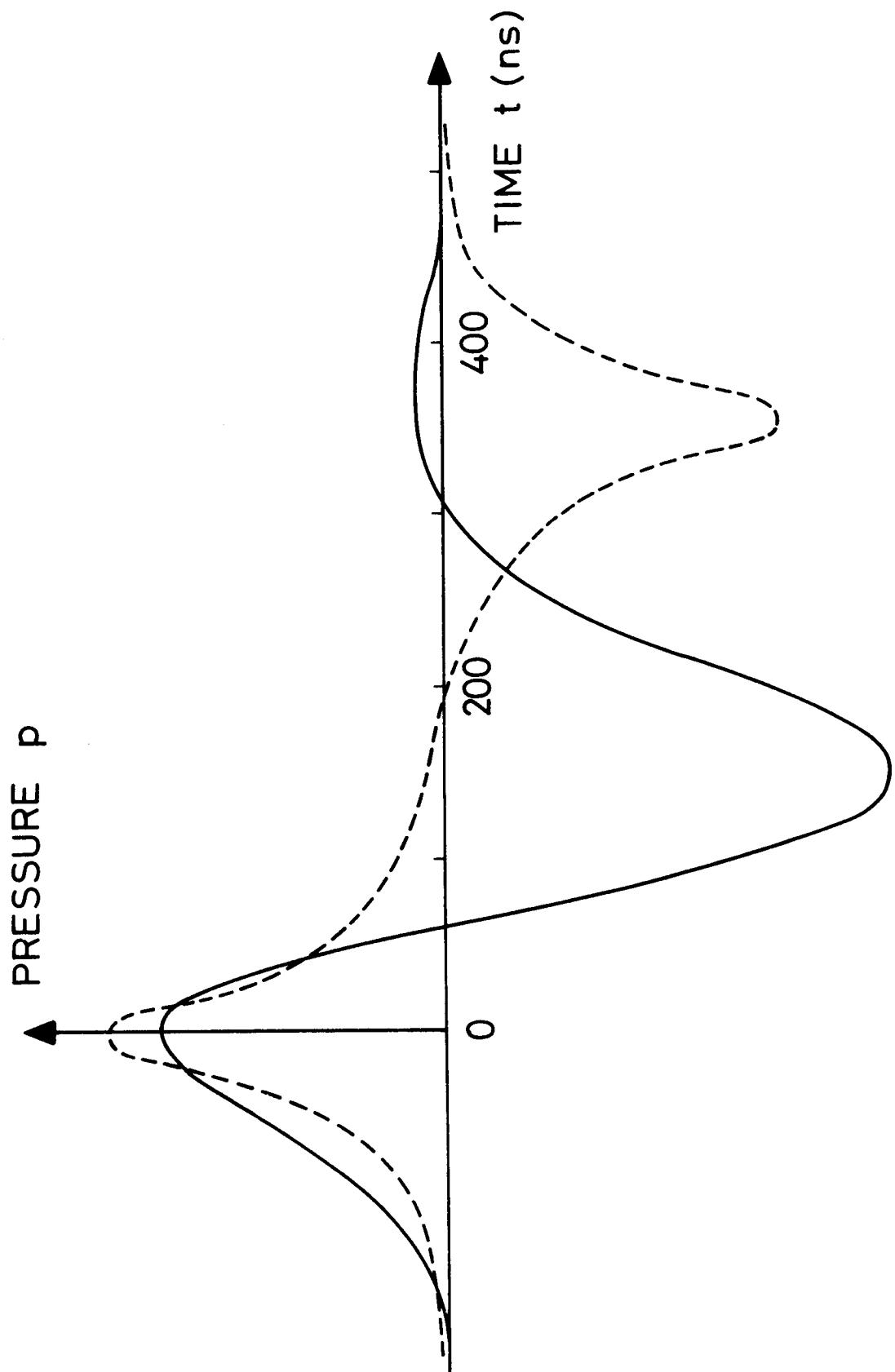


Fig.13

PART II: A SPHERICAL ANALYTICAL MODEL OF THERMOELASTIC
ACOUSTIC WAVE GENERATION IN LIQUIDS

I. INTRODUCTION

Previous theories treat the pure thermoelastic generation of stress waves mainly in one dimension [1, 2, 3, 4, 5] . Carome et al. [1] , Gournay [2] and White [3] gave a one-dimensional linear analytical solution for acoustic waves of small amplitude. These models show, that the time dependence of a laser-induced thermoelastic pressure wave in a liquid depends on the surface condition of the liquid. For the laser impact on a free surface, a symmetric pressure signal with respect to the time axis is predicted.

On the contrary, only a compressive pulse with higher amplitude is expected for the impact on a confined surface. In the following we are only interested in the case of a free surface, corresponding to our experimental conditions.

In contrast to these analytical one-dimensional models that are valid only for small amplitudes, Bushanam et al. [6] published numerical results for waves with finite and large amplitude.

Their computer code allows the treatment of plane, cylindrical and spherical waves.

In Part I , Chapter V E , we already mentioned that only Hu [7] described an analytical solution for thermoelastic waves of spherical geometry. In his model the transient heat source is approximated by a rectangular laser pulse in time with a duration of t_L . According to Hu, no analytical solution of the problem is obtainable, if the heat source follows a Gaussian distribution in space. This heat source is represented by the absorbed laser energy density in the liquid. Consequently, Hu had to assume the following, non-Gaussian dependence of the laser power P on the radius r across the laser beam:

$$\begin{aligned} P &= 1 && \text{for } r \leq a , \\ P &= e^{-\gamma(r-a)} && \text{for } r > a , \end{aligned}$$

where a represents the focal radius of the laser beam, and γ is a shape constant.

In Part I , Chapter V E , we have discussed the inadequacy of Hu's model for the thermoelastic acoustic wave. In the following we wish to present an analytical model which gives good agreement with the experiment.

II. BASIC EQUATIONS AND BOUNDARY CONDITIONS

The description of the acoustic waves generated by the thermoelastic effect can be derived on the basis of the Navier-Stokes equation (1) , the equation of volume dilatation (2) and of the equation of heat conduction (3) :

$$\rho \cdot \frac{d^2 \vec{u}}{dt^2} \approx \rho \cdot \frac{\partial^2 \vec{u}}{\partial t^2} = - \text{grad } p \quad , \quad (1)$$

$$\text{div } \vec{u} = \Delta V/V = - p/B + \beta \theta \quad , \quad (2)$$

$$\frac{\partial \theta}{\partial t} = + \kappa \cdot \Delta \theta \quad . \quad (3)$$

The following notations have been used in these equations:

- \vec{u} displacement vector,
- V particle volume,
- p pressure disturbance created by the thermoelastic wave,
- B bulk modulus
- β cubic thermal expansion coefficient,
- ρ density,
- θ excessive temperature,
- κ thermal diffusivity.

In Eq. (2) nonlinear terms are neglected. This restricts the model to waves with small amplitudes which are observed experimentally in the case of the pure thermo-elastic process. Gournay [2] and White [3] used the one-dimensional form of Eq. (2) , whereas Hu reduced this equation to $p = -B \operatorname{div} \vec{u}$.

Furthermore, the attenuation of sound due to the viscosity of the liquid and due to the influence of the heat conduction is neglected. This assumption imposes the following restrictions on the parameters of the problem [8] :

$$r_o \gg \kappa/C \quad , \quad r_o \gg \sqrt{\kappa t_L} \quad , \quad c^2 \cdot t_L \gg \kappa \quad , \\ c^2 \cdot t_L \gg \eta \quad ,$$

where r_o = typical focal radius,
 t_L = duration of the laser pulse,
 η = kinematic viscosity,
 C = sound speed.

These conditions are within the scope of our investigations.

From Eqs. (1) and (2) the following wave equation for \vec{u} can be deduced:

$$\Delta \vec{u} - \frac{1}{C^2} \frac{\partial^2 \vec{u}}{\partial t^2} = \beta \cdot \text{grad } \theta, \quad (4)$$

$$\text{where } C = (B/\rho)^{1/2}$$

Carome et al. [1] , Gournay [2] , White [3] , Cleary et al. [4] and Bushnell et al. [5] used the one-dimensional form of this equation.

Since the spatial temperature gradient is the driving force of the wave represented by Eq. (4) , the thermoelastic process is effective mainly for short laser pulses.

For spherical geometry we put $\vec{u} = \vec{u}(r,t)$, where r is the distance from the impact, which is equal to the radius of the wave. The boundary conditions are

$$\vec{u}(r,t) = 0 \quad \text{for } r \rightarrow \infty, \quad (5)$$

at all times

$$\left. \begin{aligned} \vec{u}(r,t) &= 0 \\ \frac{\partial \vec{u}(r,t)}{\partial t} &= \vec{v}(r,t) = 0 \end{aligned} \right\} \begin{aligned} &\text{at } t = 0 \text{ for} \\ &\text{any point in space.} \end{aligned} \quad (6)$$

Note that $\vec{v}(r,t)$ represents the particle velocity at the point r and at time t .

Since only longitudinal waves propagate in liquids, it follows $\text{rot } \vec{u} = 0$, yielding $\vec{u}(r,t) = \text{grad } \Phi(r,t)$, where $\Phi(r,t)$ is called the displacement potential function. In accordance with Hu's theory, Eq. (4) can therefore be transformed into

$$\Delta_r \Phi(r,t) - \frac{1}{c^2} \frac{\partial^2 \Phi(r,t)}{\partial t^2} = \beta \theta(r,t), \quad (7)$$

where

$$\Delta_r \Phi(r,t) = \frac{\partial^2 \Phi(r,t)}{\partial r^2} + \frac{2}{r} \frac{\partial \Phi(r,t)}{\partial r}.$$

The integration constant has been adjusted to zero.

Consequently, the boundary conditions (5) and (6) become

$$\frac{\partial \Phi(r,t)}{\partial r} = 0 \quad \text{for } r \rightarrow \infty \quad \text{at all times} \quad (8)$$

$$\left. \begin{array}{l} \Phi(r,t) = 0 \\ \frac{\partial \Phi(r,t)}{\partial t} = 0 \end{array} \right\} \quad \text{at } t = 0 \text{ for any point in space.} \quad (9)$$

Here $\frac{\partial \phi(r,t)}{\partial t}$ represents the velocity potential of the particle.

The temperature distribution $\theta(r,t)$ is determined by the equation of heat conduction only. This assumption is justified, since the influence of the stress of the acoustic wave on the temperature distribution is negligible.

III. THE HEAT POLE

In our model of thermoelastic stress generation, the heat source $\theta(r,t)$ is represented by the three-dimensional heat pole [9] , which corresponds to a solution of Eq. (3) :

$$\theta_p(r,t) = \frac{E_a}{\rho\sigma(4\pi\kappa t)^{3/2}} \cdot \exp(-r^2/(4\kappa t)) \quad , \quad (10)$$

where E_a = absorbed laser energy,

ρ = density and

σ = specific heat of the liquid.

The reflection of 10.6 μm radiation from a liquid surface is negligibly small and therefore neglected. Hence, E_a is equal to the incident energy E .

For the actual case of laser heating, we assume the temperature distribution $\theta(r,t) = \theta_p(r,t+\tau)$, where τ is related to the radius r_0 of the heat source by $4\cdot\kappa\cdot\tau = r_0^2$. At the time $t = 0$, $\theta(r,t)$ represents a Gaussian distribution in space proportional to $\exp(-r^2/r_0^2)$. This distribution corresponds to the TEM_{00} mode of the incident laser beam [10, p. 149] . In contradiction to Hu's statement, we are able to obtain an analytical solution of the wave equation for this case.

No information on the time dependence of the laser pulse is contained in our theory. Hence, the model refers to short laser pulses. The transient character of the thermoelastic process has been emphasized in the discussion of the generation of 60 MHz waves (Part I , Chapter V B) .

IV. SOLUTION OF THE WAVE EQUATION

The wave equation (7) is first solved for the temperature distribution $\theta_p(r,t)$ of Eq. (10) . This solution, called $E(r,t)$, is different from the final solution $\Phi(r,t)$ that refers to $\theta(r,t)$. Thus, Eq. (7) becomes

$$\begin{aligned} & \frac{\partial^2 E(r,t)}{\partial r^2} + \frac{2}{r} \frac{\partial E(r,t)}{\partial r} - \frac{1}{c^2} \frac{\partial^2 E(r,t)}{\partial t^2} \\ &= \frac{\beta E_a}{\rho\sigma(4\pi\kappa t)^{3/2}} \cdot \exp(-r^2/(4\kappa t)) \end{aligned} \quad (11)$$

with the boundary conditions (8) and (9) for $E(r,t)$ in mind.

Eq. (11) can be solved by using the Laplace transformation L in order to dispose of the time dependency. Consequently, Eq. (11) is transformed into

$$\begin{aligned} & \frac{\partial^2 \xi(r,s)}{\partial r^2} + \frac{2}{r} \frac{\partial \xi(r,s)}{\partial r} - \frac{s^2}{c^2} \xi(r,s) \\ &= \frac{\beta E_a}{4\pi\rho\sigma\kappa r} \cdot \exp(-r\sqrt{s}/\sqrt{\kappa}) \end{aligned} \quad , \quad (12)$$

where $\xi(r,s) \equiv L [E(r,t)]$ with the initial conditions (9) for $E(r,t)$ taken into account. The condition (8) becomes $\text{grad } \xi(r,s) = 0$ at $r \rightarrow \infty$.

Eq. (12) is of the type of an inhomogeneous Bessel differential equation. For the following we take

$[\beta E_a / (4\pi\rho\kappa\sigma)] = A = \text{constant}$. The homogeneous equation yields the two independent solutions

$$(1/\sqrt{r}) \cdot J_{-1/2}(isr/C) \quad \text{and} \quad (1/\sqrt{r}) \cdot Y_{-1/2}(isr/C) ,$$

where $J_{-1/2}(x)$ and $Y_{-1/2}(x)$ are the Bessel functions of the first and second kind, respectively. A particular solution $\xi(r,s)$ of the inhomogeneous Eq. (12) is obtained by transformation of the general formula given by Kamke [11] :

$$\begin{aligned} \xi(r,s) &= \\ &= \pi/(2\sqrt{r}) \cdot Y_{-1/2}(isr/C) \cdot \int J_{-1/2}(isr/C) \cdot \sqrt{r} \cdot A \cdot \exp(-\sqrt{s}r/\sqrt{\kappa}) \cdot dr \\ &- \pi/(2\sqrt{r}) \cdot J_{-1/2}(isr/C) \cdot \int Y_{-1/2}(isr/C) \cdot \sqrt{r} \cdot A \cdot \exp(-\sqrt{s}r/\sqrt{\kappa}) \cdot dr \end{aligned} \quad (13)$$

Integration of (13) yields [12]

$$\xi(r,s) = (A/r) \cdot \frac{\exp(-\sqrt{s}r/\sqrt{\kappa})}{(s/\kappa - s^2/C^2)} \quad (14)$$

Applying the inverse Laplace transformation [13] to

Eq. (14) , one obtains the time-dependent solution $E(r,t)$:

$$E(r,t) = \frac{Ak}{r} \cdot \left\{ \operatorname{Erfc} \frac{r}{2\sqrt{\kappa t}} - \frac{1}{2} e^{\frac{C^2}{\kappa} t} \times \left[e^{\frac{rC}{\kappa}} \cdot \operatorname{Erfc} \left(\frac{r}{2\sqrt{\kappa t}} + \frac{C\sqrt{t}}{\sqrt{\kappa}} \right) + e^{-\frac{rC}{\kappa}} \cdot \operatorname{Erfc} \left(\frac{r}{2\sqrt{\kappa t}} - \frac{C\sqrt{t}}{\sqrt{\kappa}} \right) \right] \right\} \quad (15)$$

in which $\operatorname{Erfc} x \equiv (2/\sqrt{\pi}) \cdot \int_x^\infty e^{-t^2} dt$.

This solution corresponds to the case where the heat pole $\theta_p(r,t)$ and the acoustic wave start together at $t = 0$.

We now replace $E(r,t)$ by $E(r,t+\tau)$, which represents a particular solution of Eq. (11) with $\theta(r,t) = \theta_p(r,t+\tau)$ on the right hand side. The final solution $\Phi(r,t)$ which satisfies the initial and boundary conditions (8) and (9) is then given by

$$\Phi(r,t) = E(r,t+\tau) + \Psi(r,t) \quad (16)$$

$\Psi(r,t)$ implies the general solution of the homogeneous wave equation, thus

$$\Psi(r,t) = (1/r) \cdot \{F(r-Ct) + G(r+Ct)\} \quad (17)$$

$\Psi(r, t)$ can be determined by considering the conditions (8) and (9):

$$\frac{\partial \Phi(r, t)}{\partial r} = \frac{\partial E(r, t+\tau)}{\partial r} + \frac{\partial \Psi(r, t)}{\partial r} = 0 \quad (18)$$

for $r \rightarrow \infty$ at all times.

$$\left. \begin{aligned} \Phi(r, 0) &= \Psi(r, 0) + E(r, \tau) = 0 \\ \frac{\partial \Phi}{\partial t}(r, 0) &= \frac{\partial \Psi}{\partial t}(r, 0) + \frac{\partial E}{\partial t}(r, \tau) = 0 \end{aligned} \right\} \quad (19)$$

for any point in space.

The following $\Psi(r, t)$ fulfils the above conditions:

$$\begin{aligned} \Psi(r, t) &= -\frac{A\kappa}{2r} \cdot \operatorname{Erfc}\left(\frac{r-Ct}{2\sqrt{\kappa\tau}}\right) - \frac{A\kappa}{2r} \cdot \operatorname{Erfc}\left(\frac{r+Ct}{2\sqrt{\kappa\tau}}\right) \\ &+ \frac{A\kappa}{2r} \cdot \exp(C^2\tau/\kappa - C(r-Ct)/\kappa) \cdot \operatorname{Erfc}\left(\frac{r-Ct}{2\sqrt{\kappa\tau}} - \frac{C\sqrt{\tau}}{\sqrt{\kappa}}\right) \\ &+ \frac{A\kappa}{2r} \cdot \exp(C^2\tau/\kappa + C(r+Ct)/\kappa) \cdot \operatorname{Erfc}\left(\frac{r+Ct}{2\sqrt{\kappa\tau}} + \frac{C\sqrt{\tau}}{\sqrt{\kappa}}\right) \end{aligned} \quad (20)$$

V. THE PRESSURE

If Eq. (2) is solved for $p(r,t)$, remembering
 $\vec{u}(r,t) = \text{grad } \Phi(r,t)$, the result can be substituted into
the wave equation (7) , yielding

$$p(r,t) = - \rho \cdot \frac{\partial^2 \Phi(r,t)}{\partial t^2} \quad (21)$$

Keeping in mind Eq. (16) , Eq. (21) can also be written in
the form as

$$p(r,t) = - \rho \cdot \left(\frac{\partial^2 \Xi(r,t+\tau)}{\partial t^2} + \frac{\partial^2 \Psi(r,t)}{\partial t^2} \right) . \quad (22)$$

With $\Xi(r,t)$ from Eq. (15) , taken at $t + \tau$, and $\Psi(r,t)$ from Eq. (20) , we find after a lengthy calculation:

$$\begin{aligned}
 p(r,t) = & - \frac{A\rho\kappa}{2r} \cdot \frac{C^3}{\sqrt{\pi\tau} \kappa^{3/2}} \cdot \left[e^{-\frac{(r-Ct)^2}{4\kappa\tau}} - e^{-\frac{(r+Ct)^2}{4\kappa\tau}} \right] \\
 & - \frac{A\rho C^4}{2r\kappa} \cdot e^{-\frac{C}{\kappa}(r-C(t+\tau))} \cdot \operatorname{Erfc}\left(\frac{r-Ct}{2\sqrt{\kappa\tau}} - \frac{C\sqrt{\tau}}{\sqrt{\kappa}}\right) \\
 & - \frac{A\rho C^4}{2r\kappa} \cdot e^{+\frac{C}{\kappa}(r+C(t+\tau))} \cdot \operatorname{Erfc}\left(\frac{r+Ct}{2\sqrt{\kappa\tau}} + \frac{C\sqrt{\tau}}{\sqrt{\kappa}}\right) \\
 & + \frac{A\rho\kappa C^2}{2\sqrt{\pi} [\kappa(t+\tau)]^{3/2}} \cdot e^{-\frac{r^2}{4\kappa(t+\tau)}} \\
 & + \frac{A\rho C^4}{2r\kappa} \cdot e^{+\frac{C}{\kappa}(r+C(t+\tau))} \cdot \operatorname{Erfc}\left(\frac{r}{2\sqrt{\kappa(t+\tau)}} + \frac{C\sqrt{t+\tau}}{\sqrt{\kappa}}\right) \\
 & + \frac{A\rho C^4}{2r\kappa} \cdot e^{-\frac{C}{\kappa}(r-C(t+\tau))} \cdot \operatorname{Erfc}\left(\frac{r}{2\sqrt{\kappa(t+\tau)}} - \frac{C\sqrt{t+\tau}}{\sqrt{\kappa}}\right)
 \end{aligned}$$

(23)

Since in our case the arguments of Erfc are either large positive or large negative, the expansions of Erfc x into continued fractions [14] yield

$$\text{Erfc } x \approx \frac{1}{(\sqrt{\pi}x)} \cdot \exp(-x^2) \quad \text{for } x \gg 0 \quad (24)$$

$$\text{Erfc } x \approx 2 + \frac{1}{(\sqrt{\pi}x)} \cdot \exp(-x^2) \quad \text{for } x \ll 0 \quad (25)$$

Introducing (24) and (25) in Eq. (23) and neglecting all terms containing $\exp(-x^2)$ with $x \geq 50$, we find

$$p(r,t) = \frac{A\rho\kappa}{2\sqrt{\pi}r} \cdot \exp \left[-(r-Ct)^2/r_o^2 \right] \times \left\{ \frac{C^4}{\kappa^2} \cdot \frac{1}{\left(\frac{C\sqrt{\tau}}{\sqrt{\kappa}} - \frac{r-Ct}{2\sqrt{\kappa\tau}} \right)} - \frac{C^3}{\kappa^{3/2} \cdot \sqrt{\tau}} \right\} \quad (26)$$

Since $C\sqrt{\tau}/\sqrt{\kappa} \gg (r-Ct)/(2\sqrt{\kappa\tau})$, the expression $1/\left(\frac{C\sqrt{\tau}}{\sqrt{\kappa}} - \frac{r-Ct}{2\sqrt{\kappa\tau}}\right)$ can be written as $(\sqrt{\kappa}/C\sqrt{\tau}) + (r-Ct) \cdot \kappa/(2C^2\tau\sqrt{\kappa\tau})$.

Introducing the constant $A = [\beta \cdot E_a / (4\pi\rho\kappa\sigma)]$, one obtains the relevant expression

$$p(r,t) = - \frac{\beta E_a C^3}{2\pi^{3/2} \sigma r_o^3} \cdot \frac{1}{r} \cdot \left(t - \frac{r}{C}\right) \cdot e^{- \left[\frac{C}{r_o} \left(t - \frac{r}{C}\right) \right]^2}$$

(27)

This function is plotted in Fig. 1 (dashed curve) for water and for $r_0 = 1.6 \cdot 10^{-4}$ m , with the aid of a Hewlett-Packard computer (Model 9821A) in conjunction with a plotter (Model 9862A) .

Fig. 1 shows that $p(r,t)$ consists of a positive pulse followed by a symmetric negative pulse. The positive peak is reached already at the time $t = r/C - r_0 / (\sqrt{2}C)$ and not at $t = r/C$ where it would be expected.

The reason for this is that in our model the acoustic wave starts at $r = r_0/\sqrt{2}$ at time $t = 0$. This distance is equal to the radius of the flex point of the Gaussian curve, which represents the starting temperature distribution.

VI. COMPARISON WITH THE EXPERIMENT

The two peak amplitudes are given by Eq. (27)

$$p_{\max} = -p_{\min} = \frac{\beta \cdot E_a \cdot c^2 \cdot e^{-1/2}}{(2\pi)^{3/2} \cdot \sigma \cdot r_o^2 \cdot r} \propto \frac{E_a}{r_o^2} \cdot \frac{1}{r} \quad (28)$$

The calculated peak pressures p_{\max} are similar to those obtained from the model of Hu. However, they are in general higher than the measured peak pressures by a factor of two to three. Two reasons are made responsible for this discrepancy. First, the stress transducers were not calibrated dynamically. Second, we have already pointed out in Part I, that the energy contained in the long tail of the laser pulse does not contribute to the thermoelastic effect. The same argument applies to the fact that the peak pressures are not proportional to the laser pulse energy E , but to $E - E_o$, for $E > E_o$. This has been verified experimentally with $E_o = 13$ mJ for water. For higher laser energies, this discrepancy is meaningless. This is in agreement with the experiments by Botygina et al. [15] performed with a Nd-laser and water. These authors obtained $p \propto E_a$ with $60 \text{ J} \leq E_a \leq 160 \text{ J}$. Even at these high energies absorbed in the liquid, no vaporization occurred, since water has a low absorption coefficient α of approximately 0.4 cm^{-1} for the wavelength of the Nd-laser ($1.06 \text{ }\mu\text{m}$).

Furthermore their investigation shows, that the thermo-elastic process is extremely inefficient for long laser pulses. Botygina et al. measured similar peak pressures as ours for much higher laser energies, yet pulse durations of 1 ms .

As expected our spherical model predicts peak pressures proportional to $1/r$. This could be verified by the experiment (Part I , Fig. 9) .

The dependence of p_{\max} on the liquid is contained in the factor $\beta C^2/\sigma$ of Eq. (28) , which predicts higher values for n-heptane than for water. This is confirmed qualitatively by the experiment as is seen by comparing Figs. 8 and 11 of Part I . According to Eq. (28) , even higher peak pressures p_{\max} should be obtained for CCl_4 in contradiction to the measurements (Part I , Fig.11) .

This discrepancy is explained by the generation of additional cylindrical waves in CCl_4 . This implies that only part of the incident energy is responsible for the generation of the hemi-spherical wave.

In contrast to the theory by Hu, the calculated time dependence of the signal is in excellent agreement with the experiment. In Fig. 1 the stress signal of Fig. 7 c (Part I) , recorded in water, is compared with the corresponding computer plot of Eq. (27) , normalized to the same p_{\max} .

The time separation T between the peak-to-peak pressures follows from Eq. (27) : $T = \sqrt{2} \cdot r_0 / C$. Thus, T is proportional to the radius r_0 of the hemi-spherical heat source which approximates the laser impact. This radius r_0 is determined by both the laser spot radius and the absorptivity of the liquid. Consequently, T is not a constant, but depends on the liquid. Hence, T can be adjusted for each individual liquid, taking its absorptivity into account. With increasing absorption coefficient α of the liquid, r_0 is expected to decrease. The lower limit is given by the minimal focal radius (≈ 0.15 mm) of the laser beam. This is in agreement with our experiment, since the measured values of T (Part I , Chapter V E) are best fitted by $r_0 = 0.16$ mm for water, $r_0 = 0.4$ mm for n-heptane and $r_0 = 0.5$ mm for CCl_4 . The value for water is minimal due to its higher absorption coefficient α and vice versa for CCl_4 . Note the shorter acoustic pulse length that results for increasing α .

The correct prediction of T has been confirmed by an additional measurement, performed with a N_2 -laser. This laser provided pulses of 12 ns halfwidth, which were focused on the free surface of a mixture of water and rhodamine 6 G . The absorbed energy density was well below the vaporization threshold, so that a symmetric stress pulse, typical for the pure thermoelastic process, resulted. The recording is shown in Fig. 2 , yielding $T \approx 50$ ns in agreement with the value calculated from the lateral dimension of the laser focus of approximately 50 μm . In contradiction, Hu's theory would give $T = 12$ ns , equal to the duration of the laser pulse.

VII. CONCLUSIONS

The good agreement of our spherical model with the experimental results of thermoelastic generation of acoustic waves in liquids, demonstrates the adequate description of the laser-induced heat source by the three-dimensional heat pole. Our theory is shown to be superior to previous models with respect to both, formulation and quantitative results. Its analytical solution is applicable to various experimental conditions. These concern the transient heating, without a phase change, of liquids and solids with different physical properties, by the impact of a laser or electron beam.

REFERENCES

1. E.F. Carome, N.A. Clark and C.E. Moeller,
Appl. Phys. Lett. 4, 95 (1964)
2. L.S. Gournay,
J. Acoust. Soc. Am. 40, 1322 (1966)
3. R.M. White,
J. Appl. Phys. 34, 3559 (1963)
4. S.F. Cleary and P.E. Hamrick,
J. Acoust. Soc. Am. 46, 1037 (1969)
5. J.C. Bushnell and D.J. Mc Closkey,
J. Appl. Phys. 39, 5541 (1968)
6. G.S. Bushanam and F.S. Barnes,
J. Appl. Phys. 46, 2074 (1975)
7. C.L. Hu,
J. Acoust. Soc. Am. 46, 728 (1969)
8. F.V. Bunkin and V.M. Komissarov,
Sov. Phys. Acoust. 19, 203 (1973)
9. A. Sommerfeld, Partielle Differential-
gleichungen der Physik
(Dieterich'sche Verlagsbuchhandlung
Wiesbaden, 1947), Vol. VI .

10. W.W. Duley, CO₂ Laser: Effects and Applications
(Academic Press, New York, San Francisco and London, 1976)
11. E. Kamke, Differentialgleichungen
(Akademische Verlagsgesellschaft, Leipzig 1967),
Vol. I .
12. I.S. Gradshteyn and I.W. Ryzhik,
Table of Integrals, Series and Products
(Academic Press, New York and London, 1965)
13. A. Erdély, W. Magnus, F. Oberhettinger and
F.G. Tricomi,
Tables of Integral Transforms
(Mc Graw-Hill Book Company, Inc., New York,
Toronto and London, 1954), Vol. I .
14. M. Abramowitz and I.A. Segun,
Handbook of Mathematical Functions
(Dover Publications, Inc., New York, 1968)
15. N.N. Botygina, V.I. Bukatyi and
S.S. Khmelevtsov,
Sov. Phys. Acoust. 22, 368 (1976)

FIGURE CAPTIONS

- Fig. 1 Theoretical thermoelastic acoustic wave according to our model (dashed curve) superimposed on the experimental record (solid curve).
- Fig. 2 Thermoelastic acoustic wave in a mixture of water and rhodamine 6G , generated by the impact of a N_2 -laser pulse of 12 ns halfwidth.

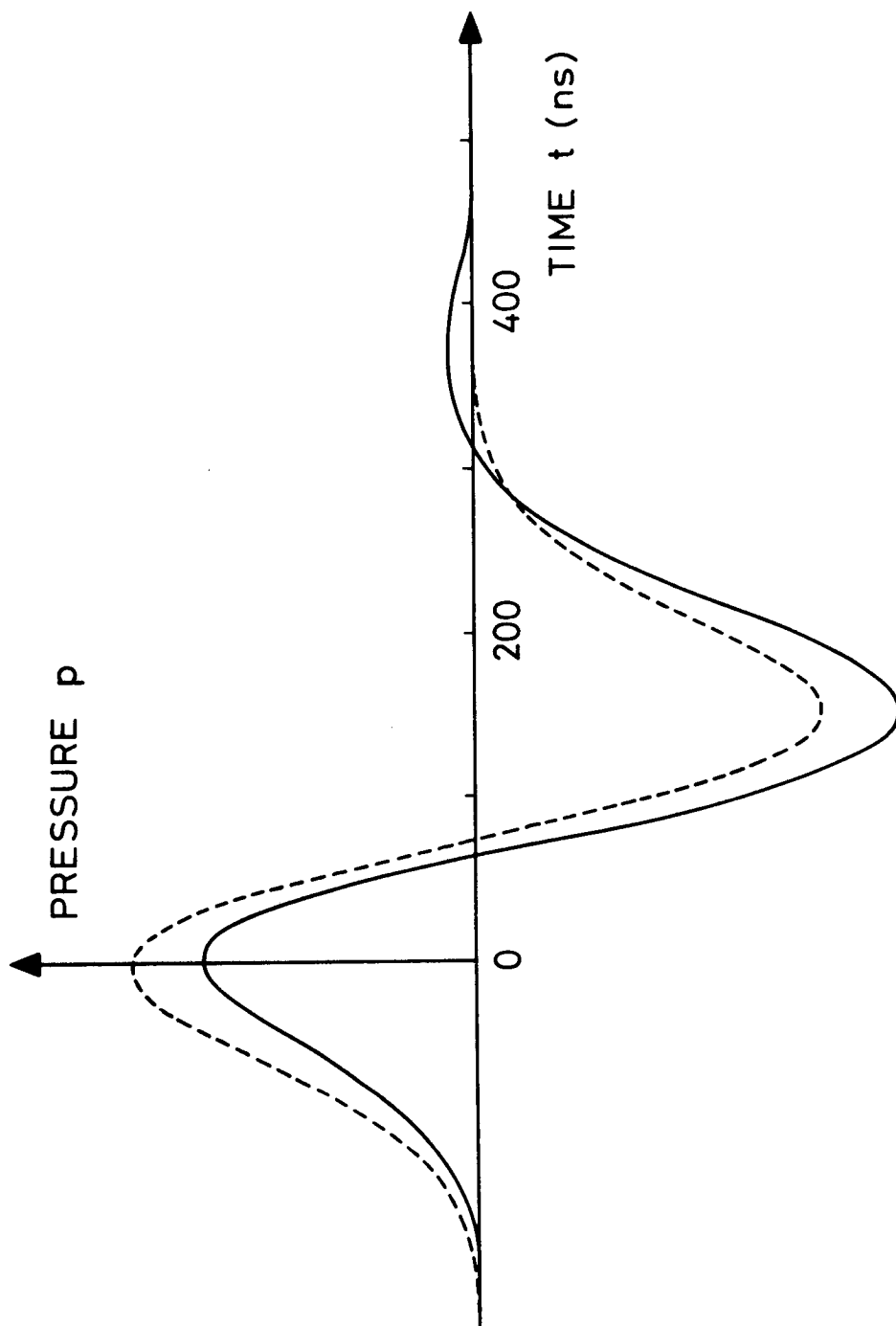


Fig. 1

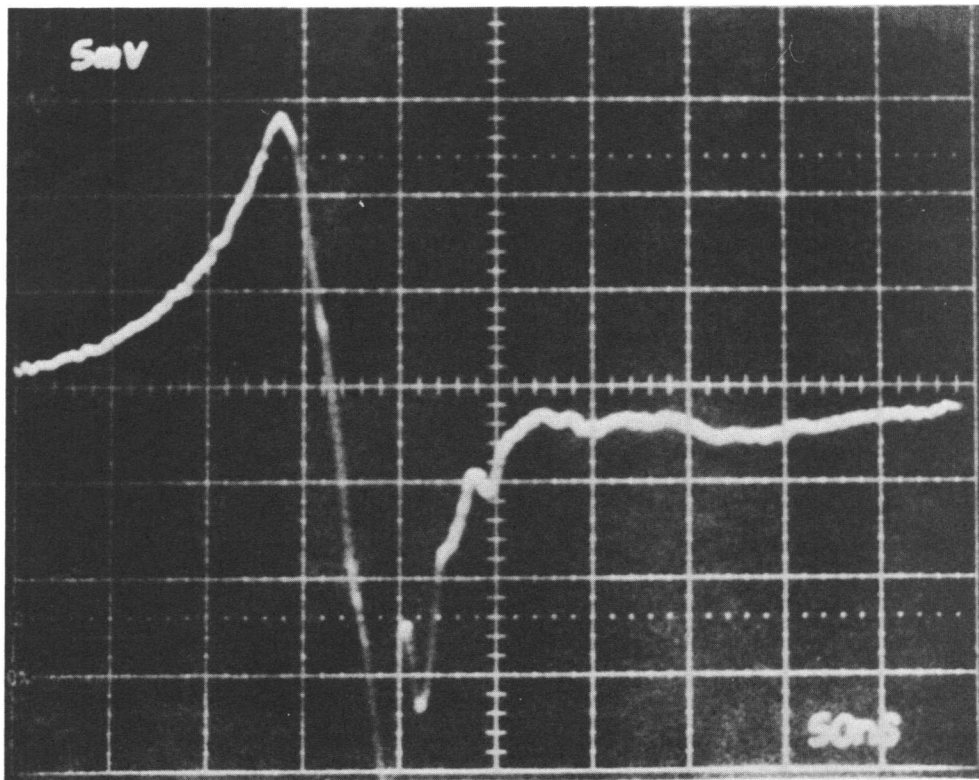


Fig. 2

ACKNOWLEDGEMENTS

I am very grateful to Prof. Dr. F. Kneubühl (ETH Zurich) for his active support and inspiration of my work and to Prof. Dr. H.P. Weber (Berne), Dr. D.C. Emmony (Loughborough), Dr. S. Witkowski (Garching), Dr. C. v. Kessel (Eindhoven), Prof. Dr. W. Lukosz (ETH Zurich) and Prof. Dr. N. Rott (ETH Zurich) for fruitful discussions.

I am also indebted to Prof. Dr. E. Stiefel and F. Spirig of the Department of Mathematics of the ETH Zurich for their active help in mathematical problems as well as to Prof. Dr. F. Aebi (GRD Thun) for lending the IMACON camera.

A part of the experiments were performed with the help of F. Fuchs, P. Herrmann and Ch. Sturzenegger.

Furthermore, I wish to thank for their support:

B. Adam, Ch. Allemann, Mrs. M. Bischof, W. Borer, U. Martens, A. Michalitsanos, Miss Ch. Noll, E. Treichler and H. Vogt, H. Wuest and M. Zazzeri.

Curriculum vitae

I was born in Illnau, Canton Zurich, on the 6th September 1948 as a citizen of Rafz ZH. I attended the primary and secondary schools in Illnau until spring 1963 . After four and a half years at the Cantonal High School in Wetzikon ZH I passed the examination "Maturität Typus C" in autumn 1967 and entered as a student the Department of Mathematics and Physics of the Swiss Federal Institute of Technology in Zurich. I received the Diploma in Physics in spring 1972 . Since May 1972 I have been working as assistant under the guidance of Prof. Kneubühl at the Solid State Physics Laboratory, where I was engaged in the research on laser interaction with condensed matter.